



29 Greater changes where permafrost exists supports the notion that increased
30 soil thaw is shifting hydrological contributions to more subsurface flow. The
31 manifestations of warming, hydrological cycle intensification, and permafrost
32 thaw will impact Arctic terrestrial and coastal environments through altered
33 river flows and the materials they convey.

34 1 Introduction

35 Hydrological cycle intensification and permafrost thaw are among a myriad of
36 environmental changes reshaping the Arctic environment (Rawlins et al., 2010; Hinz-
37 man et al., 2013; Box et al., 2019; Overland et al., 2019). Climate forcings including
38 increasing air temperature and precipitation are key drivers of alterations to the
39 Arctic system (Box et al., 2019). The Arctic has warmed 2.5 to 4 times faster
40 than the global average over the past several decades (Rantanen et al., 2022; Wang
41 et al., 2022) and experienced substantial decreases in Arctic Ocean sea ice extent
42 and volume (Stroeve and Notz, 2018; Serreze and Meier, 2019). Warming is lead-
43 ing to hydrologic intensification that is projected to drive higher precipitation rates
44 (Bintanja and Selten, 2014; McCrystall et al., 2021), with concomitant rises in river
45 discharge (Shiklomanov and Shiklomanov, 2003; Dankers and Middelkoop, 2008).
46 Permafrost thaw has the potential to change how water is stored and moved, and
47 to mobilize vast stores of organic carbon sequestered in soils (Frey and Smith, 2005;
48 Koch et al., 2022; Mohammed et al., 2022), and rising river discharge (Peterson et al.,
49 2002; Wagner et al., 2011; Feng et al., 2021) furthermore imply associated changes
50 in exports of water, energy, carbon, and other constituents to coastal zones (Tank
51 et al., 2016; Behnke et al., 2021; Zhang et al., 2021). In light of these alterations, it
52 is important to better understand how climate warming, hydrological cycle intensi-
53 fication, and permafrost thaw will impact Arctic terrestrial hydrology and, in turn,
54 exports of freshwater and associated materials through the Arctic drainage basin and
55 into coastal zones.

56 The seasonal storage of precipitation in the form of snow is a defining element
57 of Arctic hydrology, contributing to abundant surface water storages and high river
58 flows following spring melt. The presence of permafrost is another important element
59 influencing the region's water cycle. Climate warming is intensifying Earth's water
60 cycle, increasing precipitation, evaporation, evapotranspiration (ET), and river dis-
61 charge globally (Huntington, 2006, 2010), and across Arctic regions (Peterson et al.,
62 2002; Déry et al., 2009; Rawlins et al., 2010). Intensification or "acceleration" in-
63 volves the effects of both atmospheric moisture holding capacity and moisture avail-
64 ability. Declining sea ice is making the Arctic Ocean and its surrounding seas a



65 more available source of moisture, with locally-driven precipitation recycling great-
66 est in winter across the Beaufort-Chukchi, Laptev, Kara, and East Siberian Seas
67 (Ford and Frauenfeld, 2022). Increasing late summer precipitation and a shift to-
68 ward rainfall runoff is occurring across watersheds in northwest Alaska (Arp et al.,
69 2020; Rawlins, 2021; Arp and Whitman, 2022). Terrestrial hydrology in the Arctic
70 is also strongly controlled by the presence of permafrost and the seasonal thawing
71 and freezing of soils (Tananaev et al., 2020). Permafrost underlies approximately
72 one fifth of the global land area and influences processes involving runoff, aquatic
73 biogeochemistry (Frey and McClelland, 2009; Spencer et al., 2015; Hu et al., 2023),
74 and land-atmosphere greenhouse gas exchanges (Christensen et al., 2004; McKenzie
75 et al., 2021). Permafrost acts as an impermeable hydrological barrier, helping to
76 maintain high soil suprapermfrost moisture levels while reducing soil water storage
77 capacity and constraining subsurface flow (Woo et al., 2008; Walvoord and Kurylyk,
78 2016). The presence or absence of permafrost and variability in precipitation pro-
79 cesses lead to varying amounts of surface and subsurface runoff contributions to river
80 discharge and, in turn, land-ocean exports of freshwater and associated materials.
81 Warming is causing long-term changes in near-surface soil freeze/thaw cycles and
82 permafrost (Anisimov and Reneva, 2006; Koven et al., 2013; Guo et al., 2018; Peng
83 et al., 2018; Biskaborn et al., 2019), with implications for permafrost hydrology (Woo
84 et al., 2008; Liljedahl et al., 2016; Lafrenière and Lamoureux, 2019; Jin et al., 2022).
85 Subsidence due to thawing soils will likely lead to more runoff, while significantly
86 accelerating drying of tundra landscapes in a warming climate (Painter et al., 2023).
87 Studies suggest that permafrost degradation leads to increased moisture transport
88 from the surface to deeper soils, potentially contributing to increased river baseflows
89 (Walvoord and Striegl, 2007) and cold season discharge (St. Jacques and Sauchyn,
90 2009; Shiklomanov et al., 2013; Tananaev et al., 2016; Rawlins et al., 2019; Debolskiy
91 et al., 2021; Wang et al., 2021; Liu et al., 2022). In northwest Alaska, positive trends
92 in air temperature and precipitation are greatest in autumn which, together with
93 permafrost thaw, is likely leading to enhanced subsurface “suprapermfrost” runoff
94 during that time (Rawlins, 2021).

95 Climate models are essential tools for understanding how manifestations of cli-
96 mate warming will alter the Arctic’s terrestrial hydrology and riverine land-ocean
97 fluxes. Model projections point to future precipitation increases over the 21st century
98 through enhanced regional evaporation and poleward moisture transport (Bintanja
99 et al., 2020), and sea ice declines (Bintanja and Selten, 2014). Models with the
100 strongest warming response point to decreased snowfall across the high (70–90 °N)
101 Arctic. The precipitation increases are firmly linked to Arctic warming and sea-ice
102 decline (Bintanja, 2018; Arp et al., 2020), and are likely to increase river discharge



103 (Peterson et al., 2002; Zhang et al., 2013). Recent coordinated research programs
104 have produced bias-corrected climate model data for historical and future condi-
105 tions from consistent protocol frameworks (Warszawski et al., 2014; Lange, 2021).
106 Simulations of permafrost dynamics and associated soil freeze-thaw processes require
107 attention to several key processes absent in many land-surface models (Alexeev et al.,
108 2007; Nicolsky et al., 2007; Lawrence and Slater, 2008). Slater and Lawrence (2013)
109 concluded that, in general, permafrost is not well represented by the ensemble of
110 CMIP5 models. Examining permafrost dynamics in global models participating in
111 the CMIP6, Burke et al. (2020) found that simulation of active-layer thickness (ALT)
112 and other key features often fell outside the observed range, with errors attributable
113 to shallow and poorly resolved soil profiles and structural weaknesses in snow physics
114 and soil hydrology within some of the models.

115 In this study we use simulations with a permafrost hydrology model to evaluate
116 how climate alterations linked to warming, primarily hydrological cycle intensifica-
117 tion and permafrost thaw, will influence Arctic terrestrial hydrology and, in turn,
118 land-ocean riverine freshwater and biogeochemical fluxes. We begin by examining
119 meteorological data from climate models to understand the atmospheric forcings
120 and their influence on surface hydrology. Model simulations are validated against
121 select observations for sublimation, ET, ALT, and river discharge. We then examine
122 changes over the 21st century to gain insights into how hydrological cycle intensifica-
123 tion and permafrost thaw are impacting key elements of Arctic terrestrial hydrology
124 controlling river exports, and test the hypothesis that within the Arctic drainage
125 basin, changes in subsurface runoff are greatest in permafrost areas.

126 **2 Methods**

127 **2.1 Study area and spatial grid**

128 The pan-Arctic drainage basin used in this study encompasses approximately
129 22.45 million square kilometers. It has a wide range of land cover types, from grass-
130 lands in southern Canada and central Eurasia to boreal forests to tundra in far
131 northern areas. This domain includes basins of rivers draining to the Arctic Ocean,
132 Hudson Bay, and the Bering Strait, with the large Yukon River draining into the lat-
133 ter. The region's four largest rivers—the Ob, Yenesej, Lena, and Mackenzie—flow
134 primarily in a south-to-north direction, and account for roughly half (49%) of the
135 pan-Arctic basin area. Model forcing data, simulations, and outputs were produced
136 on the 25×25 km EASE-Grid (Brodzik and Knowles, 2002), with 35,693 gridcells
137 covering the study spatial domain.



138 2.2 Modeling approach

139 The modeling approach leverages simulations with the Permafrost Water Balance
140 Model (PWBM v4) to investigate the impacts of warming, hydrological cycle intensi-
141 fication, and permafrost thaw on terrestrial hydrological fluxes within and through
142 the pan-Arctic drainage basin. The PWBM simulates all major elements of the water
143 cycle, including transpiration and soil and surface-water evaporation, snow storage,
144 sublimation (Rawlins et al., 2003, 2013), runoff (Rawlins et al., 2021), and soil freeze-
145 thaw. Past applications include assessment of causes behind record Eurasian dis-
146 charge (Rawlins et al., 2010); estimation of surface water dynamics (Schroeder et al.,
147 2010); analysis of present and future water budgets (Clilverd et al., 2011); quantifi-
148 cation of freshwater and dissolved organic carbon fluxes (Rawlins et al., 2021); inves-
149 tigation of trends in those fluxes to a coastal lagoon in northwest Alaska (Rawlins,
150 2021); and exploration of the links between surface organic soil properties and mois-
151 ture dynamics across the Alaska North Slope (Yi et al., 2022). PWBM operates at an
152 implicit daily time step, with meteorological forcings (air temperature, precipitation,
153 wind speed) typically drawn from reanalysis data for regional-scale simulations or,
154 when applied to smaller watersheds, meteorological station data. Daily simulated ET
155 depends on atmospheric demand and surface and soil conditions. The model includes
156 a surface water pool that is typically transient and most often occurs after snowmelt.
157 The sum of surface and subsurface runoff from one or more soil layers within a grid-
158 cell constitutes daily total runoff. We use the term “subsurface runoff” for the water
159 flux often called “baseflow”, which is water seeping into the stream from groundwa-
160 ter. Subgrid fraction of inundated area (lakes and ponds) are parameterized based
161 on observed data (Du et al., 2016), with total runoff across each gridcell calculated
162 as a weighted total from the inundated and non-inundated areas. The snow model
163 simulates the effects of seasonal changes in snow density and, in turn, snow ther-
164 mal conductivity (Liston et al., 2007; Sturm et al., 1995). Soil freeze-thaw process
165 representations include a multi-layer soil module with algorithms for unfrozen water
166 dynamics and phase change, as well as specification of the thermal and hydrological
167 properties of organic soils (Sazonova and Romanovsky, 2003; Nicolsky et al., 2007).
168 The PWBM has a 60 meter soil column, includes parameterizations for thermal and
169 hydraulic properties of organic soils, and simulates the effect of depth hoar and wind
170 compaction on snow density. Rawlins et al. (2013) describe the soil freeze-thaw and
171 snow algorithms, and calibration procedures, which involve factors controlling ET,
172 snow sublimation, and subsurface runoff that differ between forest and tundra land-
173 scapes. In this study each transient simulation was preceded by a 50-year spinup on
174 year 1980 to stabilize soil temperature, moisture, and soil dissolved organic carbon
175 (DOC) pools. While parameterizations for fields such as soil texture and vegetation



176 cover are fundamental elements of land surface and hydrological model simulations,
177 simulated runoff in Arctic regions is most sensitive to the time-varying meteorological
178 forcings (Rawlins et al., 2003).

179 Permafrost extent is based on end of season soil temperatures. If the soil column
180 down to the maximum 60 meter depth is frozen, beneath a thawed upper zone (i.e.
181 active layer), the gridcell is deemed to have permafrost that year. The impact of
182 subsidence on permafrost thaw is not accounted for in the simulations, though the
183 effect may be relatively small (Painter et al., 2023). In models operating at continen-
184 tal scales, estimates of permafrost extent across transition zones between continuous
185 permafrost and the non-permafrost areas are more uncertain due to limitations re-
186 solving spatial variations.

187 2.3 Meteorological forcings

188 This study focuses on numerical model simulations that were forced with grid-
189 ded meteorological data (Table 1). We begin by examining simulations forced with
190 reanalysis data to characterize dynamics over the recent past. Changes over the 21th
191 century are assessed using simulations forced with meteorological data from coupled
192 climate models, rather than the hydrology (eg. runoff) from them, as outputs from
193 individual models can vary widely, and often imply unrealistic long-term systematic
194 changes in water storage and level within entire basins (Bring et al., 2015).

Table 1: Simulations conducted in the study, time period for the transient simulation, and origin of forcing data. Each transient simulation was preceded by a 50 year spinup. For the climate model forcing, the 1980–2100 period includes two different experiments.

Model simulations		
Name	Period	Forcing
PWBM-W5E5	1980–2019	Bias-adjusted ECMWF Reanalysis v5 (ERA5)
PWBM-ERA5	1980–2019	ERA5 Reanalysis
PWBM-MERRA	1980–2013	Modern-Era Retrospective Analysis for Research and Applications
PWBM-IPSL	1980–2100	IPSL-CM6A-LR (Historical: 1980–2014, SSP3-7.0: 2015–2100)
PWBM-MPI	1980–2100	MPI-ESM1-2-HR (Historical: 1980–2014, SSP3-7.0: 2015–2100)



195 Simulations were made using forcings from three reanalysis datasets (W5E5,
196 ERA5, MERRA) and two global climate models from the Coupled Model Inter-
197 comparison Project Phase 6 (CMIP6). The WFDE5 data—WATCH Forcing Data
198 methodology applied to ERA5 reanalysis—is bias-adjusted ERA5 data at $0.5^\circ \times 0.5^\circ$
199 spatial and sub-daily resolutions, generated specifically to be used as climate data in-
200 puts for impacts studies (Cucchi et al., 2020). The WFDE5 over land is merged with
201 ERA5 over the ocean to produce W5E5 data (Lange, 2019), compiled as part of phase
202 3b of the Inter-Sectoral Impact Model Intercomparison Project (ISIMIP3b) (Lange,
203 2019, 2021). We downloaded and analyzed W5E5 version 2 data for use as meteoro-
204 logical forcings for simulations over the historical period. We use bias-adjusted data
205 (W5E5 v2 and climate models) prepared as part of the ISIMIP framework (Cucchi
206 et al., 2020; Lange et al., 2021). We also applied data from ERA5 and MERRA
207 reanalysis to gauge the accuracy of the air temperature (2 m), precipitation, and
208 wind speed forcings and for model validation. Precipitation amounts in the W5E5
209 data are lowest among the three reanalysis datasets. To ameliorate this bias in the
210 simulation forced with W5E5 we increased each precipitation value by 20%. The
211 ISIMIP3b climate model forcing data are bias adjusted and statistically downscaled,
212 and available for five CMIP6 models (GFDL-ESM4, IPSL-CM6A-LR, MPI-ESM1-
213 2-HR, MRI-ESM2-0, UKESM1-0-LL) forced with three Shared Socioeconomic Path-
214 ways (SSP) scenarios (SSP1-2.6, SSP3-7.0, SSP5-8.5). In our two simulations over
215 years 1980–2100 we used data from two models (MPI-ESM1-2-HR, IPSL-CM6A-LR)
216 forced with SSP3-7.0, which is a high emissions scenario, and suitable to investigate
217 the response of Arctic hydrology to a strong climate forcing. These two climate
218 models generally bracket the range of climate projections for the pan-Arctic region
219 across the five CMIP6 models (Fig. S1). The selection of these two models—hereafter
220 IPSL and MPI—is aimed at capturing a wide range of temperature and precipita-
221 tion projections, but not necessarily the full range. Air temperature and precipita-
222 tion changes expressed by the models are described in Sect. 4.1 and 4.2 respectively. In
223 a study examining which CMIP3 models performed best at capturing meteorological
224 quantities across parts of the Arctic, a predecessor of the MPI-ESM ranked highest
225 (Walsh et al., 2008).

226 2.4 Statistical analysis

227 Our analysis of changes closely connected to Arctic rivers centers on differences
228 between 20-yr intervals representing early (2000–2019) and late (2080–2099) cen-
229 tury conditions. Specifically we mapped climatological averages over these periods
230 and examined the differences for each domain gridcell. Domain-wide averages were



231 computed from all 35,693 gridcells covering the domain. The statistical significance
232 of differences between the two periods were calculated for select quantities. Before
233 applying the statistical significance test we used graphical analysis and the Shapiro–
234 Wilk test (Shapiro and Wilk, 1965) to determine if the data series of interest is
235 approximately normally distributed. The paired t test was then applied to test the
236 null hypothesis that the mean difference between two variables is zero. Relative (per-
237 centage) difference is calculated based on the standard formula: Relative difference
238 (%) = $(Z_2 - Z_1) / Z_1 \times 100$, where Z_1 and Z_2 are values for early and late periods
239 respectively. In this study we leverage these simulations forced by the two climate
240 models to investigate the sensitivity of thermal and hydrological responses to dif-
241 ferent climate forcings, not to provide robust quantitative projections, which would
242 require a multi-model, multi-scenario ensemble.

243 3 Model Validation

244 We first compared key components of the simulated water budget–active-layer
245 thickness, sublimation, evapotranspiration, and discharge–with different observa-
246 tional datasets to assess the credibility of the PWBM simulations. Simulated active-
247 layer thickness (ALT) and model-estimated permafrost extent is compared to ALT
248 data from the National Tibetan Plateau/Third Pole Environment Data Center (TPDC)
249 (Fig. 1a–c) and permafrost area from International Association of Permafrost (IPA)
250 data. Simulated ALT in the model simulations spans a greater range compared with
251 the TPDC data (Fig. 1d). However, the TPDC ALT estimates are known to have a
252 reduced distribution range owing to the machine learning approach used (Ni et al.,
253 2021). Permafrost extent is generally well captured, with differences from total area
254 of continuous and discontinuous permafrost in the IPA dataset of less than 10%
255 (Table 2).

256 We used the simulation forced with W5E5 data (PWBM-W5E5) to evaluate the
257 magnitude of vertical fluxes of water from sublimation and ET over the recent past
258 (Fig. 2). Overestimates in simulated sublimation are noted (domain-wide average
259 sublimation of 40 mm yr^{-1} for GLEAM and 57 mm yr^{-1} for PWBM-W5E5), though
260 the discrepancy is small relative to the magnitudes of annual total runoff and ET.
261 Simulated ET (260 mm yr^{-1}) falls between the estimates from GLEAM (304 mm
262 yr^{-1}) and remote sensing-based data (230 mm yr^{-1}), differences of 14% and 12%
263 respectively. The model generally captures the spatial pattern in sublimation and
264 ET.

265 We compared simulated discharge volume to a new dataset, the Remotely-sensed
266 Arctic Discharge Reanalysis (RADR), that was generated through assimilation of ap-

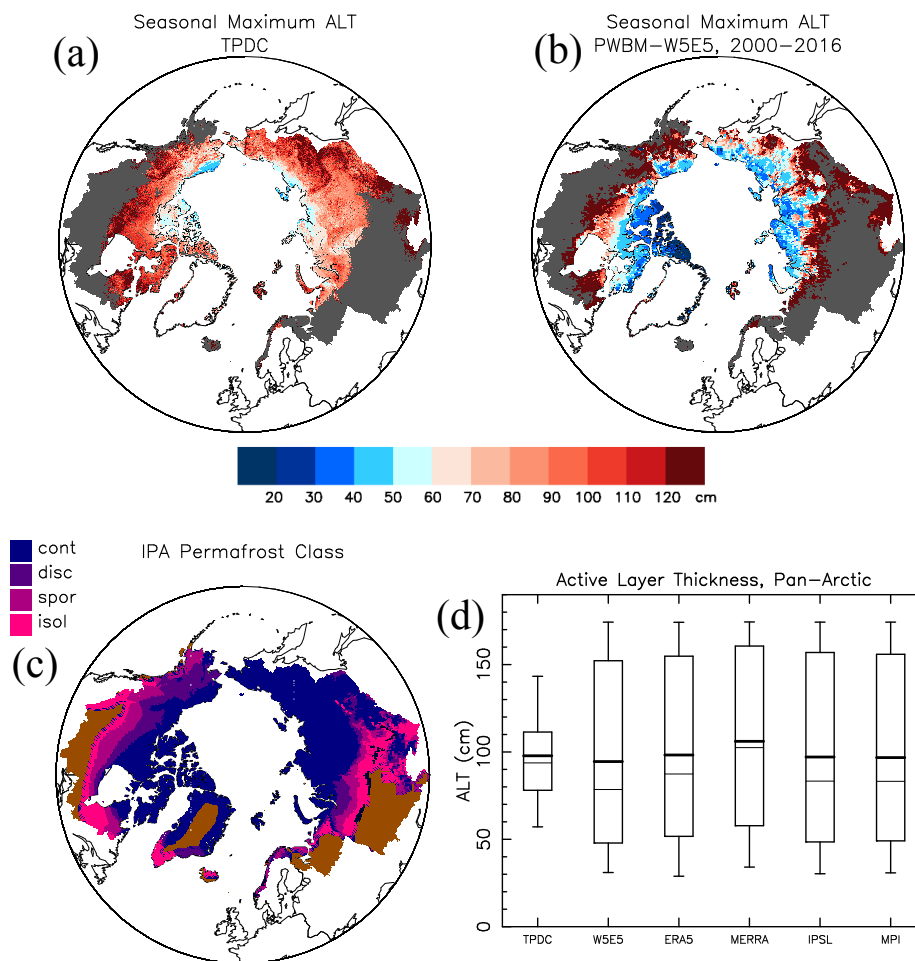


Figure 1: (a) Active-layer thickness (ALT, cm) from the TPDC database (Ran et al., 2022) for the period 2000–2016, and (b) from the PWBM simulation forced with W5E5 data over same period. Grey shading indicates non-permafrost areas. (c) Permafrost classification from International Association of Permafrost (IPA) data. (d) Distributions of seasonal maximum ALT (cm) for all grids with permafrost. ALT is the average for each year over the period 2000–2016. TPDC is used as validation for the ALT estimated by simulations forced with data from W5E5, ERA5, MERRA (2000–2013), IPSL, and MPI. Boxplot rectangles bracket the 25th and 75th percentiles. Whiskers extend to the 5th and 95th percentiles. Thick and thin horizontal lines mark the distribution mean and median respectively



Table 2: Permafrost areal extent and difference from observed extent across the study domain. Area in million km² from the International Permafrost Association (IPA) classification (Brown et al., 2001), the National Tibetan Plateau Data Center (TPDC) dataset (Ran et al., 2022), and PWBM simulations. Areas of continuous and discontinuous permafrost were added for the IPA estimate. Difference is defined based on observations from the IPA-based extent. For the simulated estimates, a gridcell is deemed to have permafrost under the standard definition of ground (model soil layer) that remains at or below 0°C for at least 2 consecutive years.

Data	Area (10 ⁶ km ²)	Difference (%)
IPA	13.2	–
TPDC	12.5	–5.5
PWBM-W5E5	12.7	–4.2
PWBM-ERA5	13.1	–0.8
PWBM-MERRA	10.5	–20.4
PWBM-IPSL	12.4	–6.2
PWBM-MPI	11.8	–10.9

267 proximately 9.18 million discharge observations derived from 227 million river width
268 measurements from Landsat images (Feng et al., 2021). Simulated discharge vol-
269 ume is the sum total of runoff over the contributing river basin. This evaluation
270 was performed for total discharge from the pan-Arctic drainage basin and five large
271 Arctic rivers: the Ob, Yenesej, Lena, Mackenzie, and Yukon (Fig. S2). The model
272 tends to overestimate discharge across western Eurasia and underestimate it across
273 eastern Eurasia. Differences are modest for the two North American rivers. Yet the
274 magnitude of pan-Arctic discharge is well constrained. Average freshwater export
275 to the Arctic Ocean from the study domain over the period 1984–2018 is 5,169 km³
276 yr^{–1} based on RADR. Over the same period, annual total discharge is 5752, 5822,
277 and 5811 km³ yr^{–1} in the simulations forced by W5E5, IPSL, and MPI respectively
278 (Fig. S3), giving differences from RADR discharge of less than 13%. The simulation
279 forced with W5E5 captures the acceleration in Arctic discharge reported in other
280 studies (Peterson et al., 2002; Feng et al., 2021). The linear trend of 8.3 km³ yr^{–2}
281 (0.15% yr^{–1}) closely aligns with the acceleration (11.6 km³ yr^{–2}, 0.22% yr^{–1}) from
282 RADR discharge (Feng et al., 2021), and is in the upper range of estimates (3.5–
283 10 km³ yr^{–2}) from prior studies (Shiklomanov et al., 2000; McClelland et al., 2006;
284 Rawlins et al., 2010). For comparison, an analysis for the four largest Arctic-draining
285 rivers (Mackenzie, Ob, Yenisei, and Lena) indicates that the combined annual dis-
286 charge increased by 89 km³ decade^{–1} over the period 1980–2009, amounting to an
287 approximate 14% increase over the 30-year period (Ahmed et al., 2020). Hydrologi-
288 cal cycle intensification is connected with warming, and also manifested by increases

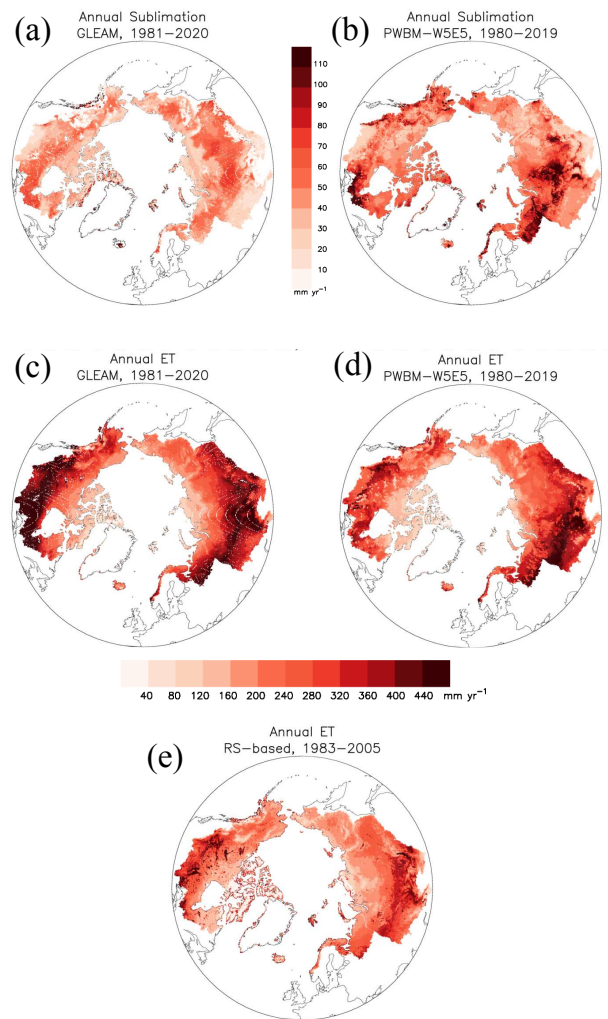


Figure 2: (a) Annual total sublimation (mm yr⁻¹) and (c) evapotranspiration (ET, mm yr⁻¹) from GLEAM (Miralles et al., 2011; Martens et al., 2017) and PWBM-W5E5 (b,d). Bottom panel (e) shows ET from a dataset derived from remote sensing data (Zhang et al., 2009).

289 in vertical fluxes of precipitation and ET. The differences of less than 15% between
290 model simulated ET and discharge, and the estimates from the validation datasets,



291 suggests that the water budget components are sufficiently well constrained to enable
 292 evaluation of the impact of climate warming on runoff and river discharge in Arctic
 293 rivers. In general, the comparisons with observations support the model’s ability to
 294 reliably simulate key hydrological variables of interest.

295 4 Alterations connected to hydrological cycle in- 296 tensification and permafrost thaw

297 4.1 Air temperature

298 In this analysis we use the simulations forced by the two climate models to bracket
 299 changes likely to occur this century, focusing primarily on twenty-year periods repre-
 300 senting early (2000–2019) and late (2080–2099) century conditions. The IPSL model
 301 projects stronger warming compared to MPI, with warming between early and late
 302 century of 7.2 °C (domain-wide mean value) and 6.2 °C, respectively (Table 3). Both
 303 show the strongest warming over the highest latitudes of the pan-Arctic basin, with
 304 warming of over 10 °C across far northern Canada projected by IPSL. More modest
 305 warming of 3–4 °C is noted over southwestern Canada and central Eurasia in the
 MPI data.

Table 3: Climatological averages for early (2000–2019) and late (2080–2099) century periods from the simulations forced with IPSL and MPI meteorological data. ^aRelative (percentage) difference shown for each except air temperature, which is shown in degrees C. Differences are statistically significant for all quantities listed based on the paired T test (Sect. 2.4).

Variable	PWBM-IPSL			PWBM-MPI		
	early	late	% diff ^a	early	late	% diff ^a
air temp (C)	−5.3	1.9	7.2	−5.3	−0.9	6.2
precipitation (mm yr ^{−1})	578	697	21	573	643	12
net precipitation (mm yr ^{−1})	258	315	22	259	300	16
rainfall (mm yr ^{−1})	334	437	31	354	413	17
snowfall (mm yr ^{−1})	244	260	7	219	230	5
rainfall fraction (%)	56	62	11	43	63	47
runoff (mm yr ^{−1})	264	329	25	266	310	17
F _{sub} (%)	27	35	30	30	34	13

306



307 In the results that follow, unless otherwise noted, statements reporting two statis-
308 tics will be written in order for PWBM-MPI and PWBM-IPSL respectively. In nearly
309 every instance, changes are greater with the latter simulation due to the influence of
310 forcing from the more strongly warming (and wetter) IPSL climate model.

311 4.2 Precipitation

312 Rainfall rates have also been increasing across much of the pan-Arctic. Rainfall
313 will continue to increase this century, particularly along favored storm track regions
314 over northwestern Eurasia and western Alaska (Fig. 3a, S4a), where the majority of
315 water vapor transport into the Arctic occurs (Nash et al., 2018). Climatological aver-
316 age rainfall (domain average) is higher by late century, with relative differences of 17
317 and 31% for the MPI and IPSL models, respectively (Table 3). Snowfall is projected
318 to increase over a smaller geographic extent, mainly the higher latitudes and across
319 the colder parts of eastern Eurasia, and decrease over most of the pan-Arctic, most
320 prominently western Eurasia and southern Canada (Fig. 3b, S4b). The domain-wide
321 change averages 5 and 7%. The sizable rainfall increases drive the projected rise in
322 the fraction of rainfall to total precipitation (Fig. 3c, S4c) averaging 11 and 47%
323 for the two simulations. Net precipitation—the difference between precipitation and
324 the sum of evapotranspiration and snow sublimation—is projected to increase across
325 most (> 75%) of the pan-Arctic basin. Decreases will occur across southern Canada
326 and Eurasia. For areas with and without permafrost, mean changes (increases) are 31
327 and 42%, and 5 and 6%, respectively. The simulations thus reveal bigger impacts—a
328 net wetting—over permafrost regions, and a strong latitudinal south-north gradi-
329 ent in future precipitation changes that will influence river discharge quantity and
330 quality.

331 4.3 Permafrost extent and active layer thickness

332 Research studies have documented hydrological cycle intensification and per-
333 mafrost thaw across the terrestrial Arctic. To better understand changes in per-
334 mafrost hydrology attributable to warming and increasing soil thaw we calculated
335 ALT averages from the two climate-model-forced simulations (Fig. 4, S5). For
336 PWBM-IPSL, permafrost area decreases by 7.8 million km² (12.3 to 4.5 million km²)
337 from the early to late century periods, a decline of 63% of present day permafrost
338 area. For PWBM-MPI, some 4.9 million km² or 42% of present area loses permafrost
339 (11.7 to 6.8 million km²). Predictions of soil temperature from CMIP5 models point
340 to permafrost fractional losses by end of century of 15% to 87% for RCP4.5, and 30%

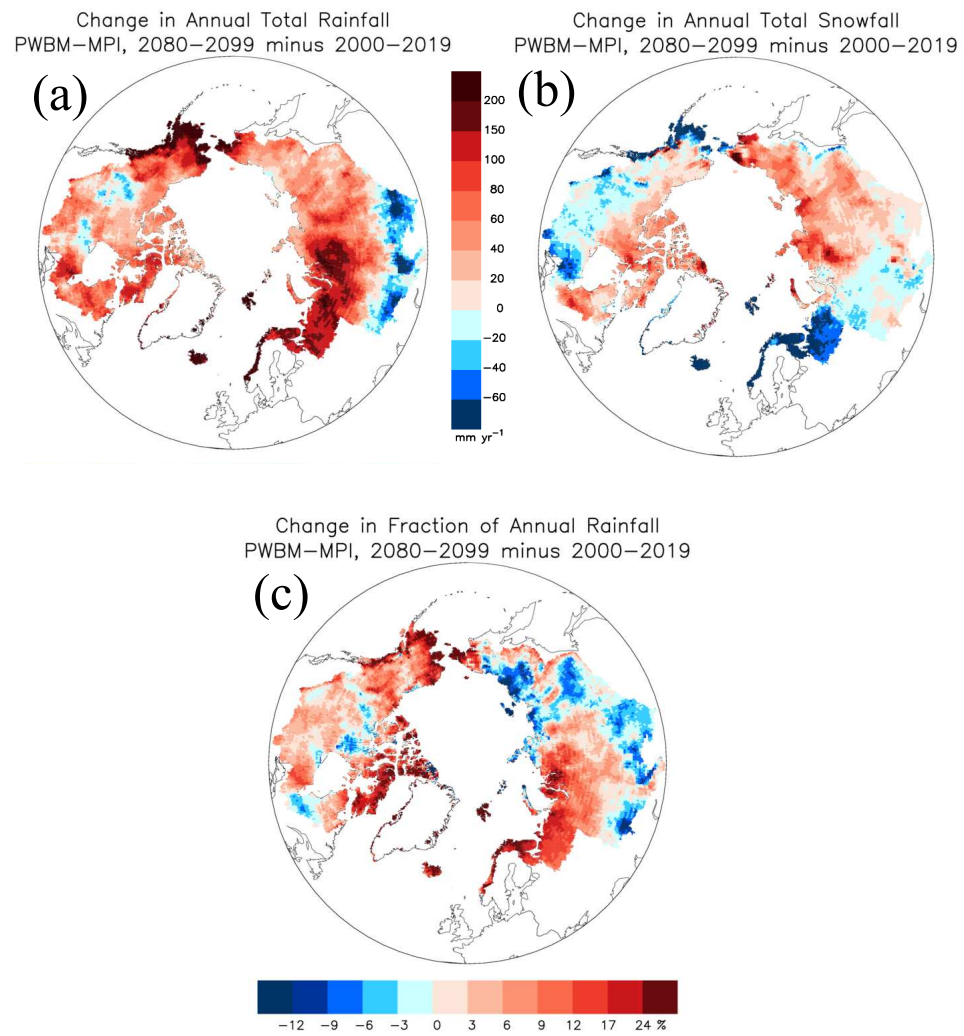


Figure 3: Change in (a) annual rainfall (mm yr^{-1}), (b) snowfall (mm yr^{-1}), and (c) the fraction of rainfall to total precipitation from PWBM-MPI simulation.

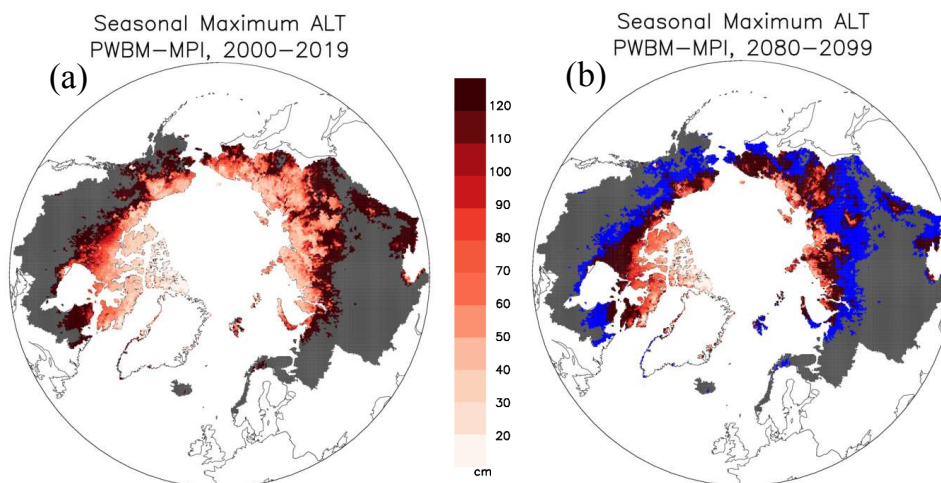


Figure 4: Simulated active-layer thickness (ALT, cm) for (a) early (2000–2019) and (b) late century (2080–2099) periods from PWBM-MPI. Blue shading highlights areas that are no longer characterized as permafrost in the future period. Gray areas are non-permafrost areas of the Arctic basin.

341 to 99% for RCP8.5 (Koven et al., 2013). Across areas that maintain permafrost, the
342 ALT increases between the two periods average 56 and 91 cm. For comparison, esti-
343 mates over permafrost areas obtained from an air temperature-based thawing index
344 applied to 16 CMIP5 models (2006–2100) forced under RCP8.5 averaged a similar
345 6.5 cm decade⁻¹.

346 4.4 Runoff and river discharge

347 Annual runoff within the pan-Arctic basin is typically highest across eastern
348 Canada, western Eurasia, and coastal regions of western Canada and western Alaska.
349 Runoff changes between the early and late century periods were calculated here to
350 assess future alterations to river discharge (Fig. 5a, S6a). In Eurasia the change in
351 annual total runoff, as a percent of the early period, is greater over northeast parts
352 of the continent. Across North America the increases are also greater in the colder
353 northern parts of the Canadian archipelago and over northern Alaska. Averaged
354 across all gridcells, annual runoff increases by 19% (45 mm yr⁻¹) and 31% (65 mm
355 yr⁻¹) from PWBM-MPI and PWBM-IPSL, respectively. Not surprisingly, the spatial
356 pattern in runoff change closely aligns with the pattern in net precipitation. There
357 is also a significant difference in the mean change in annual runoff between gridcells
358 with permafrost (67 and 99 mm yr⁻¹ increase) and those without permafrost (21 and
359 25 mm yr⁻¹). This divergence is driven by changes in net precipitation (64 and 89
360 mm yr⁻¹ vs. 18 and 19 mm yr⁻¹), as well as differing influences from deepening ALT

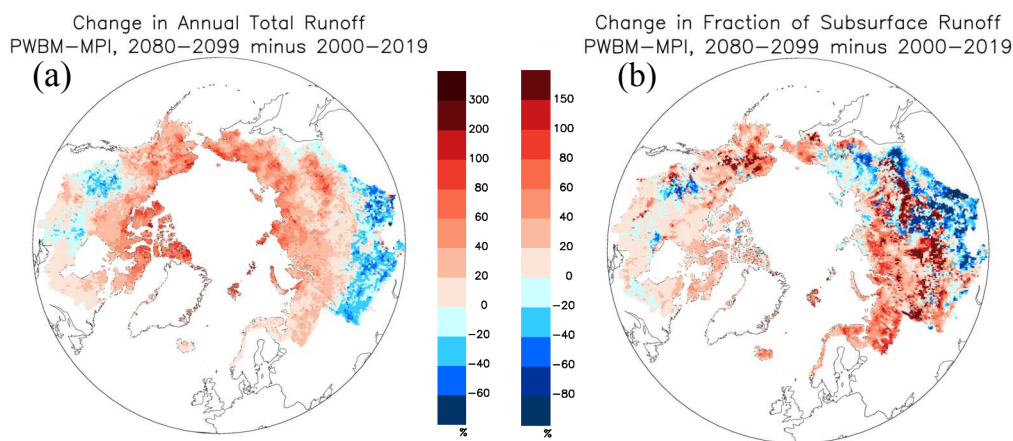


Figure 5: Change in (a) annual total runoff (%) and (b) fraction of subsurface to total runoff (F_{sub} , %) from the simulations.

361 and longer thawed periods in areas with and without permafrost. Across permafrost
362 areas, the difference between net precipitation and runoff—in a water budget, an
363 approximation for change in storage—is 3–10 mm yr⁻¹, a small amount relative to
364 the runoff increase. Over the early century period, river discharge volume is 5839,
365 5955, 5917 km³ yr⁻¹ for the PWBM-W5E5, PWBM-MPI, PWBM-IPSL simulations
366 respectively (Fig. S3). By late century, discharge volume increases to 6955 and
367 7374 km³ yr⁻¹, relative increases of 17 and 25% for PWBM-MPI, and PWBM-IPSL
368 respectively (runoff equivalents in Table 3). The trend is statistically significant (p
369 < 0.01) for both time series.

370 A transition from runoff dominated by surface water contributions toward in-
371 creasing amounts of subsurface flow is expected as the climate warms (Frey and
372 McClelland, 2009). Compared to change in total runoff, the change in the fraction
373 of subsurface to total runoff (F_{sub}) is more spatially variable across the pan-Arctic
374 (Fig. 5b, S6b). During the early century period, F_{sub} averages 30% and 27% in the
375 PWBM-MPI and PWBM-IPSL simulations respectively (Fig. 6). The fractions in-
376 crease to 34% and 35% by end of century, giving relative (percent) increase in domain
377 mean F_{sub} of 13 and 30% for PWBM-MPI and PWBM-IPSL respectively. Based on
378 the modest warming PWBM-MPI run, approximately 72% of permafrost areas will
379 have higher subsurface runoff fractions by end of century. This spatial extent in-

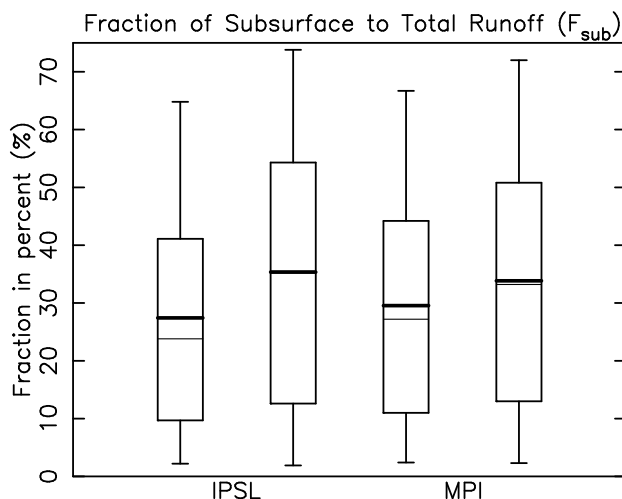


Figure 6: Fraction of subsurface to total runoff (F_{sub}) for early and late century periods for all pan-Arctic grids from PWBM-IPSL and PWBM-MPI simulations.

380 creases to 88% of the permafrost region under the more aggressive warming depicted
381 under PWBM-IPSL (Fig. S6b). The shift in F_{sub} is larger in permafrost areas, with
382 significant differences in spatial mean F_{sub} in areas with and without permafrost
383 (relative differences 15.7 and 13.5% respectively for PWBM-MPI; 31.1 and 24.4%
384 for PWBM-IPSL). The PWBM-MPI simulation reveals a significant relationship (p
385 < 0.01) between change in ALT and F_{sub} , with a 6.4% increase in F_{sub} per 0.1 m
386 increase in ALT. While the positive correlation does not exist under PWBM-IPSL,
387 the more pervasive growth in F_{sub} in PWBM-MPI suggests a connection between soil
388 thaw and increasing contributions from subsurface runoff to river discharge during
389 this century, particularly in regions underlain by permafrost.

390 The runoff changes in both simulations exhibit a significant positive relationship
391 with latitude (Fig. 7a, S7a). The linear fit suggests an additional 2.9 and 4.2% runoff
392 (PWBM-MPI and PWBM-IPSL) for each degree northward in latitude. Under this
393 pattern river discharge shifts over time to being sourced more from the northerly
394 parts of the four largest river basins (Ob, Yenesej, Lena, Mackenzie; Fig. 8a, S8a,
395 Table 4). Decreases are projected for the southerly half of the Ob, Yenesej, and
396 Mackenzie Rivers. For the Ob basin, less runoff across the southern half of the river
397 basin will be offset by higher flow in the north, so that annual total discharge exported
398 at the coast is relatively unchanged. The Yenesej shows a similar pattern, with

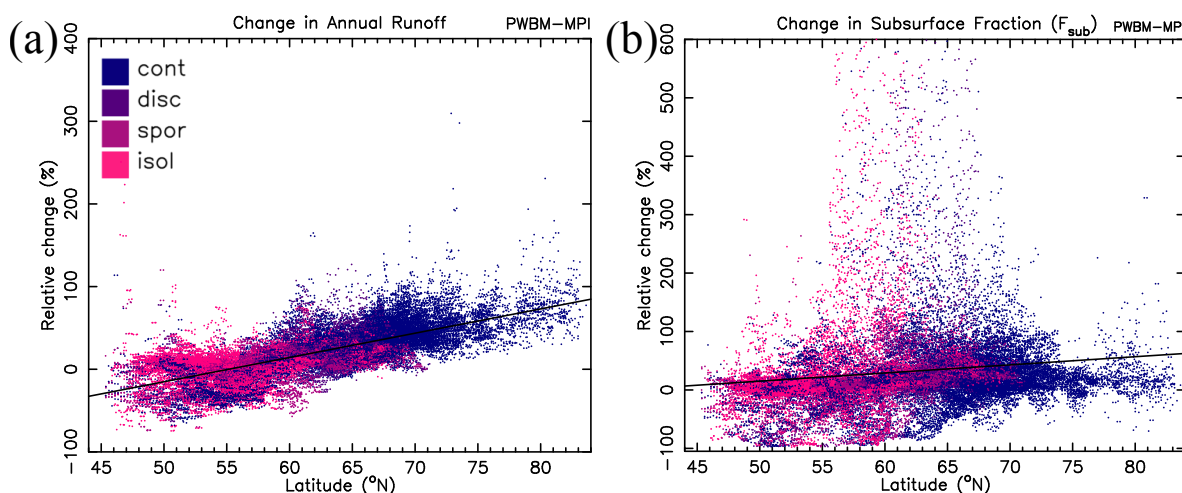


Figure 7: Change in (a) annual total runoff (%) and (b) F_{sub} with gridcell latitude from PWBM-MPI simulation for all pan-Arctic domain gridcells. Colors indicate permafrost classification for the cell from IPA (Figure 1c).

399 accumulated discharge at the coast higher by late century. The Lena and Mackenzie
400 Rivers will receive substantial additional discharge from their northern areas, with
401 the Lena projected to export 66 and $128 \text{ km}^3 \text{ yr}^{-1}$ (16 and 31%) more freshwater
402 discharge by late century. The sharp increase in export from the Yenesei and Lena
403 arising from their northern watersheds is driven primarily by higher snowfall rates
404 (Fig. 3b, S4b). Averaged across the four, the downstream half of the rivers will
405 receive approximately 20–30% more accumulated discharge from the northern half
406 of their contributing area. A south-north gradient also exists in soil carbon storage
407 in these basins, with the highest amounts in the far north (Fig. 8b, S8b). Subsurface
408 runoff increases are also greater to the north (Fig. 7b, S7b), though the scatter is
409 substantial compared to the change in annual total runoff.

410 Runoff is projected to increase during most months in both simulations (Fig. 9, S9),
411 with monthly changes remarkably similar between the two runs. Averaged over sea-
412 sons, runoff increases (depth in mm) are greatest in spring (MAM). The increase in
413 spring, particularly during May, is attributable to additional snowmelt runoff and a
414 shift to earlier snowpack melting. As a consequence, less snowmelt and runoff occur in
415 June. We applied a simple river flow accumulation and linear routing model (Rawlins
416 et al., 2019) to estimate the timing shift in discharge export at the coast. Averaged
417 across the six largest rivers (Ob, Yenesei, Lena, Mackenzie, Yukon, Kolyma), peak

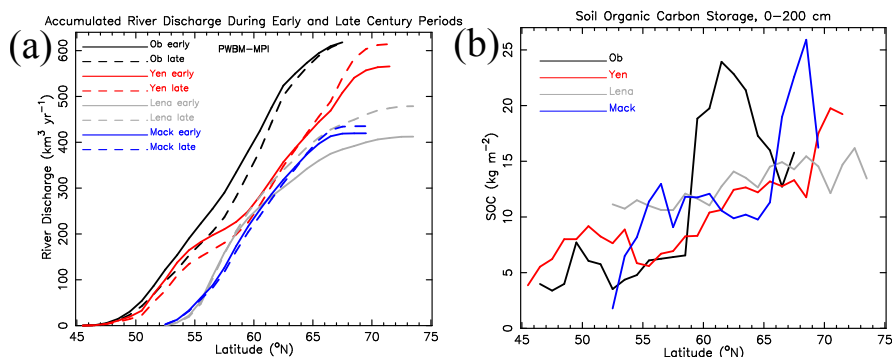


Figure 8: (a) Accumulated annual total river discharge (km³ yr⁻¹) for the Ob, Yenesei, Lena, and Mackenzie Rivers for 1° latitude bands as averages over early (solid line) and late (dashed) century periods from PWBM-MPI. (b) Soil carbon storage (kg m⁻²) in soil 0–200 cm zone from the Northern Circumpolar Soil Carbon Database (Hugelius et al., 2013).

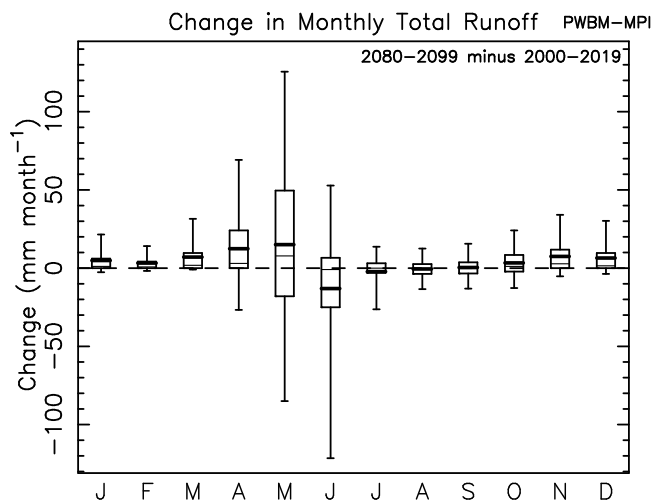


Figure 9: Distribution in change in monthly total runoff (mm month⁻¹) between early and late century periods for all pan-Arctic gridcells from PWBM-MPI.



Table 4: Relative (percentage) change in accumulated river discharge for the upstream (southern) half and downstream (northern) half of each of the four largest Arctic rivers. Averages are calculated from the totals shown in Fig.s 8, S6. Total row represents the average from the four.

River	PWBM-IPSL		PWBM-MPI	
	up (%)	down (%)	up (%)	down (%)
Ob	-9.8	7.4	-19.4	13.6
Yenesey	-1.5	27.9	-14.2	22.2
Lena	26.4	43.8	12.5	25.9
Mackenzie	-0.2	35.3	-5.3	17.3
Total	3.7	28.6	-6.6	19.7

418 daily discharge at each coastal outlet shifts earlier by end of century by approxi-
419 mately 11 days in both simulations (DOY 180 to 169 in PWBM-IPSL and DOY 176
420 to 165 in PWBM-MPI). Runoff is largely unchanged in July, August and September,
421 and the changes are not statistically significant in June and July. Seasonally, the
422 relative change (percentage change) is greatest in winter, with runoff by late century
423 a factor of 5–10 greater compared to the early century period averages. Significant
424 percentage increases are noted in autumn and spring as well. Interestingly, snow
425 storage (snow water equivalent, SWE) increases in both simulations are significant
426 in February, March, and April only. Notably, no increase in SWE is projected during
427 autumn.

428 The intensifying hydrological cycle and thawing permafrost will manifest in chang-
429 ing amounts of surface and subsurface runoff contributions to river discharge (Fig. 10).
430 The shifts vary strongly with season, and spatially across the terrestrial Arctic, with
431 remarkably similar change magnitudes in the two simulations, due largely to similar-
432 ities in patterns in net precipitation and its change this century. At the pan-Arctic
433 scale, modest increases are projected in both surface and subsurface runoff for the
434 annual total and in winter, spring, and autumn. The acceleration during winter and
435 autumn will come predominantly from additional subsurface runoff. Spring increases
436 are mainly attributable to increased surface runoff. Runoff is projected to decrease
437 slightly in summer due to less surface runoff, despite a small increase in subsur-
438 face runoff. The autumn change is particularly noteworthy over northern Alaska.
439 Also there, summer shows a strong shift from surface to subsurface runoff. Runoff
440 decreases are projected to occur in most seasons over southwest Canada, owing to
441 relatively large precipitation declines (Fig. 3, S4).

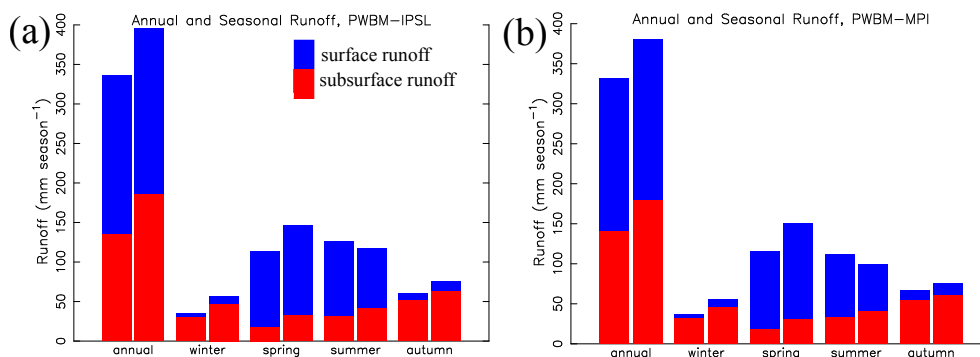


Figure 10: Annual and seasonal total runoff for the early (left bar) and late century (right bar) periods, expressed as surface (blue) and subsurface (red) amounts for (a) PWBM-IPSL and (b) PWBM-MPI simulations.

442 5 Discussion

443 The Arctic basin is drained by several rivers that receive runoff contributions
444 over great distances, from grasslands and forests in the south to tundra in the north.
445 Surface runoff has typically been a substantial component of river discharge, with
446 subsurface flows characterizing low flows in summer and early fall. These character-
447 istic patterns and dynamics are shifting due to influences from warming, primarily
448 hydrological cycle intensification and permafrost thaw. The shifts are altering the
449 water cycle from processes manifesting both horizontally, via primarily atmospheric
450 effects, and vertically, from soil thaw, and seasonally, through a combination of both
451 impacts. Recent research suggests that a warming Arctic will experience changes in
452 moisture sources that will influence freshwater exports from rivers. The two coupled
453 climate models from which outputs were used in this study capture substantial
454 precipitation increases in regions adjacent to the Arctic Ocean. This is a robust
455 feature of climate models that is linked to a more open Arctic Ocean later this cen-
456 tury (Barnhart et al., 2016; McCrystall et al., 2021). River basins near the western
457 Arctic Ocean, particularly far northeast Eurasia, northwest Canada, and northern
458 Alaska, will experience relatively large increases in river discharge, driven partly by
459 higher snowfall rates and spring SWE amounts. These are cold areas that will warm
460 significantly and, in turn, increasingly be fed by additional moisture, including from
461 more frequent atmospheric rivers (Zhang et al., 2023). In contrast, southern parts



462 of the pan-Arctic basin are projected to experience a decline in net precipitation
463 and runoff contributions to rivers. In general, rivers in central Eurasia and southern
464 Canada will receive less runoff, particularly during summer. Our results suggest that
465 nearly 90% of the increase in river discharge from permafrost regions will arise from
466 an increase in net precipitation (Cubasch et al., 2001), rather than a “de-watering”
467 of permafrost from thawing of soil ice. This connection to net precipitation is con-
468 sistent with attribution studies for the river discharge trends observed during the
469 recent past (McClelland et al., 2004, 2006). Our results point to significant shifts
470 in sources of freshwater entering Arctic rivers, with less runoff to river networks in
471 the south and more in the north. The headwaters of the large Arctic rivers like the
472 Lena, Ob, Yenisey, Mackenzie, originate well south of what is typically considered
473 Arctic lands. The simulations suggest that by end of century, some 20–30% more
474 freshwater discharge will enter, accumulate in, and be export from the northern half
475 of the four large rivers.

476 In addition to geographic shifts involving atmospheric influences, ongoing soil
477 thaw and permafrost losses will also influence runoff and materials contributions to
478 rivers. Our results support a growing body of evidence that deepening active layers
479 and losses in permafrost extent will increase subsurface runoff contributions to rivers.
480 Permafrost extent declines by 42 and 63% (PWBM-MPI and PWBM-IPSL respec-
481 tively) between early (2000–2019) and late (2080–2099) century periods, indicative
482 of recent and future permafrost degradation. Recent observations in northern Alaska
483 suggest that increased precipitation and deepening ALT play increasingly important
484 roles in sustaining low flows and enhancing subsurface hydrologic processes (Arp
485 et al., 2020; Cooper et al., 2023). Projected changes in subsurface runoff are more
486 spatially variable compared to total runoff, though a similar south-north gradient
487 exists. Increased subsurface runoff can lead to decreases in summer stream temper-
488 atures in headwater catchments (Sjöberg et al., 2021). Pronounced seasonal shifts
489 in runoff contributions will also occur. Increased runoff in late spring will likely be
490 driven by higher snow storage and earlier melt that will shift peak spring freshet
491 runoff earlier by approximately 11 days this century. Increased autumn discharge in
492 the simulations is not attributable to higher SWE, forced instead by thawing per-
493 mafrost that is lengthening the period when flow occurs, and creating deeper active
494 layers that store and release water later in the season. More runoff during November
495 and December, an approximate 5-fold increase in the modest warming simulation,
496 highlights the physical connection between warming, permafrost degradation, and
497 increasing subsurface flows to streams and rivers (St. Jacques and Sauchyn, 2009;
498 Rawlins et al., 2019). The relatively large changes in November–April runoff de-
499 scribed here are congruent with a recent study that documented a 10% per decade



500 increase in cold season discharge from nine rivers in Alaska with long data records
501 (Blaskey et al., 2023). Warming, prominent in this region during autumn and early
502 winter, can promote increased soil water storage, delaying the release of water into
503 the streams, and thus contribute to increases in winter flow (Streletskiy et al., 2015).
504 Results of this study support the hypothesis that across the Arctic basin subsurface
505 runoff increases will be greatest in permafrost areas.

506 Taken together, the spatial shifts suggest alterations in materials exported to
507 coastal waters. Warming and higher rainfall rates will enhance thaw and increase
508 coastal erosion. Higher runoff rates will drive additional subsurface contributions
509 of freshwater and DOC to coastal seas and lagoons (Connolly et al., 2020). More
510 cold season river discharge has the potential to affect sea ice dynamics and other
511 near-shore processes involving quantities such as salinity and biogeochemistry. The
512 impacts extend to water quality and materials exports by rivers. For example, DOC
513 input to the Arctic Ocean has a very high temporal and geographical variability
514 with a strong bias towards the large Eurasian Rivers and the freshet period (Amon
515 et al., 2012). Our results suggest impacts to carbon of differing quality, as Amon et al.
516 (2012) reported that lignin phenol and p-hydroxybenzene composition of Arctic river
517 DOC point to the abundance of young, boreal-vegetation-derived leachates during
518 spring flood and older, soil-, peat-, and wetland-derived DOC during groundwater
519 dominated low flow conditions. In northern tundra areas where soil carbon amounts
520 are greater, warmer temperatures and increased runoff will likely lead to increased
521 riverine DOC exports. Indeed, Frey and Smith (2005) concluded that, assuming no
522 change in either river discharge or in-channel processes, warming would produce a
523 2.7–4.4 Tg yr⁻¹ increase in terrestrial DOC flux from West Siberia to the Arctic
524 Ocean by 2100, with even larger increases likely should river discharge from the
525 region continue to increase, as depicted in the simulations examined here. Warming
526 and shifting snowmelt dynamics could increase transport and mobilization of DOC
527 as subsurface pathways become active earlier in the year (Croghan et al., 2023). In
528 contrast, some areas may experience a decrease in DOC export over time due to
529 longer flow paths and residence times, along with increased microbial mineralization
530 of DOC in the soil column (Striegl et al., 2005). Increasing soil thaw is expected to
531 accelerate the release of old carbon (Dean et al., 2018; Schwab et al., 2020), which in
532 turn will be entrained into, processed by, and exported from Arctic rivers. Moreover,
533 DOC from deep sediments (> 3 m) could also become a significant contribution
534 of carbon to Arctic rivers as the climate continues to warm (Mohammed et al.,
535 2022). Nitrate concentrations are greater at lower latitudes as compared with higher
536 latitudes where permafrost is more prominent (Frey and McClelland, 2009). Changes
537 expressed predominantly across northern parts of the Arctic basin will have a direct



538 influence on coastal zone processes. On balance, our results point to continued
539 increases in DOC export by Arctic rivers, and the mobilization and transport of
540 ancient carbon in subsurface runoff from permafrost areas.

541 The use of two climate model forcing sets increases confidence in elements of
542 the model outputs and associated analysis. It is noteworthy that results involving
543 runoff, in particular the spatial patterns, are similar between the two simulations.
544 Magnitudes of air temperature and precipitation increases are greater in the sim-
545 ulation forced with IPSL (PWBM-IPSL). Under those warmer temperatures, the
546 Hamon potential evapotranspiration function captures the temperature dependence
547 on actual and potential evapotranspiration. Higher precipitation rates in a warmer
548 forcing scenario, like IPSL, are offset by higher simulated ET, resulting in relatively
549 similar magnitudes of annual net precipitation and annual total runoff. This plausi-
550 ble modeling result suggests less uncertainty with the magnitudes of runoff changes
551 compared with the changes in meteorological forcings projected by the climate mod-
552 els. The model validation analysis suggests that the magnitude of simulated annual
553 total runoff and discharge are comparable to independent observational datasets,
554 with time trends similar in magnitude to those reported in other studies.

555 Salient conclusions from this study come with caveats related to the limits of the
556 analysis. Foremost is the large degree of uncertainty in meteorological data across
557 Arctic regions, attributable to a sparse observation network, as well as uncertain-
558 ties in the magnitude of meteorological changes projected by the two coupled climate
559 models. This uncertainty is ameliorated somewhat through the use of reanalysis data
560 and model calibration. Results are implicitly linked to the connection between land-
561 scape runoff and river discharge export. Results are also influenced by the choice of
562 climate model forced under the SSP3-7.0 scenario. In light of this, one might expect
563 lower magnitudes of change should atmospheric greenhouse gas concentrations not
564 rise to levels depicted in SSP3-7.0. The broad spatial extent and moderate model res-
565 olution (25×25 km gridcells) employed in this study limit our ability to incorporate
566 influences such as thermokarst and talik formation on runoff contributions to streams
567 and rivers. However, it is not clear that these local processes are a major component
568 of riverine materials exports by Arctic rivers (Dean et al., 2018). The model simula-
569 tions do not include interactions between lakes and the river networks, so, impacts
570 from lake thaw drainage events (Smith et al., 2005; Andresen and Lougheed, 2015;
571 Jones et al., 2022) are not simulated. The influence of land subsidence on soil temper-
572 ature, moisture, and water storage is also not simulated. While subsidence is unlikely
573 to lead to abrupt thaw over large areas, it can have significant effects on the hydrol-
574 ogy of polygonal tundra, generally increasing landscape runoff (Painter et al., 2023).
575 Our results underscore the importance in better understanding the myriad transfor-



576 mations reshaping Arctic environments. Large changes in the far north emphasize
577 the need for more frequent and spatially extensive sampling of small and medium-
578 sized rivers that ring the Arctic Ocean. Increased confidence in the magnitude of
579 likely responses will require a multi-model, multi-scenario ensemble of simulations
580 to obtain a range of projections consistent with known uncertainties. Incorporating
581 small-scale effects such as thermokarst and lake drainage on river discharge will re-
582 quire higher-resolution simulations. New model parameterization obtained from high
583 resolution remote sensing observations will improve model capabilities in simulating
584 permafrost hydrology in data sparse regions of the Arctic.

585 6 Code and data availability

586 This study is based on publicly available data for observa-
587 tions used in model validation. The W5E5 data are available at
588 <https://dataservices.gfz-potsdam.de/pik/showshort.php?id=escidoc:4855898>
589 (last access: 15 October 2022). The MERRA reanalysis data are avail-
590 able at <https://gmao.gsfc.nasa.gov/reanalysis/MERRA/> (last access: 23 Janu-
591 ary 2023). The ECMWF Reanalysis v5 (ERA5) data are available at
592 <https://www.ecmwf.int/en/forecasts/dataset/ecmwf-reanalysis-v5> (last access:
593 19 March 2023). The TPCDC data are available at <http://data.tpcdc.ac.cn/en>
594 (last access: 3 February 2023). The IPA permafrost data in the Circum-
595 Arctic Map of Permafrost and Ground-Ice Conditions, Version 2 are
596 available at <https://nsidc.org/data/ggd318/versions/2> (last access 1 Au-
597 gust 2022). The Global Land Evaporation Amsterdam Model (GLEAM)
598 data are available at <https://www.gleam.eu/> (last access: 17 April 2023).
599 The pan-Arctic ET data derived from remote sensing are available at
600 http://files.ntsg.umt.edu/data/PA_Monthly_ET/ (last access: 16 April 2023).
601 Climate model data used as forcings are available in the ISIMIP Repository
602 located at <https://data.isimip.org/>. The PWBM source code is available at
603 <https://blogs.umass.edu/csdc/pwbm/>. The climate model forcings and PWBM
604 simulation outputs are available upon request from the authors of this study.

605 7 Author contributions

606 MAR ran all the simulations, analyzed the results and wrote the paper. AVK
607 prepared the climate modeling forcing data and contributed to writing of the paper.



608 **8 Competing interests**

609 The authors declare that they have no conflict of interest.

610 **9 Acknowledgements**

611 The PWBM simulations were performed on high performance computing re-
612 sources provided by the Massachusetts Green High Performance Computing Center.
613 We are grateful to John Kimball, James McClelland, and Vladimir Alexeev and the
614 editor for their comments which have greatly improved our paper.

615 **10 Financial support**

616 This work was supported by funding from the U.S. Department of Energy, Of-
617 fice of Science, Office of Biological and Environmental Research (Grant No. DE-
618 SC0019462), the National Aeronautics and Space Administration (Grant No. 80NSSC19K0649),
619 and the National Science Foundation, Division of Polar Programs (Grant No. NSF-
620 OPP-1656026).

621 **References**

- 622 Ahmed, R., Prowse, T., Dibike, Y., Bonsal, B., and O'Neil, H.: Recent Trends in
623 Freshwater Influx to the Arctic Ocean from Four Major Arctic-Draining Rivers,
624 *Water*, 12, 1189, <https://doi.org/10.3390/w12041189>, 2020.
- 625 Alexeev, V., Nicolsky, D., Romanovsky, V., and Lawrence, D.: An evaluation of
626 deep soil configurations in the CLM3 for improved representation of permafrost,
627 *Geophys. Res. Lett.*, 34, L08501, <http://doi.org/10.1029/2007GL029536>, 2007.
- 628 Amon, R., Rinehart, A., Duan, S., Louchouart, P., Prokushkin, A., Guggenberger,
629 G., Bauch, D., Stedmon, C., Raymond, P., Holmes, R., et al.: Dissolved organic
630 matter sources in large Arctic rivers, *Geochimica et Cosmochimica Acta*, 94, 217–
631 237, <https://doi.org/10.1016/j.gca.2012.07.015>, 2012.
- 632 Andresen, C. G. and Lougheed, V. L.: Disappearing Arctic tundra ponds:
633 Fine-scale analysis of surface hydrology in drained thaw lake basins over
634 a 65 year period (1948–2013), *J. Geophys. Res.-Biogeo*, 120, 466–479,
635 <https://doi.org/10.1002/2014JG002778>, 2015.



- 636 Anisimov, O. and Reneva, S.: Permafrost and Changing Climate: The Rus-
637 sian Perspective, *AMBIO: A Journal of the Human Environment*, 35, 169–175,
638 [https://doi.org/10.1579/0044-7447\(2006\)35\[169:PACCTR\]2.0.CO;2](https://doi.org/10.1579/0044-7447(2006)35[169:PACCTR]2.0.CO;2), 2006.
- 639 Arp, C., Whitman, M., Kemnitz, R., and Stuefer, S.: Evidence of hydrological inten-
640 sification and regime change from northern Alaskan watershed runoff, *Geophys.*
641 *Res. Lett.*, 47, e2020GL089186, <https://doi.org/10.1029/2020GL089186>, 2020.
- 642 Arp, C. D. and Whitman, M. S.: Lake basins drive variation in catchment-scale runoff
643 response over a decade of increasing rainfall in Arctic Alaska, *Hydrol. Process.*,
644 36, e14583, <https://doi.org/10.1002/hyp.14583>, 2022.
- 645 Barnhart, K. R., Miller, C. R., Overeem, I., and Kay, J. E.: Mapping the
646 future expansion of Arctic open water, *Nat. Clim. Change.*, 6, 280–285,
647 <https://doi.org/10.1038/nclimate2848>, 2016.
- 648 Behnke, M. I., McClelland, J. W., Tank, S. E., Kellerman, A. M., Holmes, R. M.,
649 Haghypour, N., Eglinton, T. I., Raymond, P. A., Suslova, A., Zhulidov, A. V., Gur-
650 tovaya, T., Zimov, N., Zimov, S., Mutter, E. A., Amos, E., and Spencer, R. G. M.:
651 Pan-Arctic Riverine Dissolved Organic Matter: Synchronous Molecular Stabili-
652 ty, Shifting Sources and Subsidies, *Global Biogeochem. Cy.*, 35, e2020GB006871,
653 <https://doi.org/10.1029/2020GB006871>, 2021.
- 654 Bintanja, R.: The impact of Arctic warming on increased rainfall, *Sci. Rep.*, 8, 1–6,
655 <https://doi.org/10.1038/s41598-018-34450-3>, 2018.
- 656 Bintanja, R. and Selten, F. M.: Future increases in Arctic precipita-
657 tion linked to local evaporation and sea-ice retreat, *Nature*, 509, 479482,
658 <https://doi.org/10.1038/nature13259>, 2014.
- 659 Bintanja, R., van der Wiel, K., Van der Linden, E., Reusen, J., Bogerd,
660 L., Krikken, F., and Selten, F.: Strong future increases in Arctic precipita-
661 tion variability linked to poleward moisture transport, *Sci. Adv.*, 6, eaax6869,
662 <https://doi.org/10.1126/sciadv.aax6869>, 2020.
- 663 Biskaborn, B. K., Smith, S. L., Noetzli, J., Matthes, H., Vieira, G., Strelet-
664 skiy, D. A., Schoeneich, P., Romanovsky, V. E., Lewkowicz, A. G., Abramov,
665 A., et al.: Permafrost is warming at a global scale, *Nat. Commun.*, 10, 1–11,
666 <https://doi.org/10.1038/s41467-018-08240-4>, 2019.



- 667 Blaskey, D., Koch, J. C., Gooseff, M. N., Newman, A. J., Cheng, Y., ODon-
668 nell, J. A., and Musselman, K. N.: Increasing Alaskan river discharge during
669 the cold season is driven by recent warming, *Environ. Res. Lett.*, 18, 024042,
670 <https://doi.org/10.1088/1748-9326/acb661>, 2023.
- 671 Box, J. E., Colgan, W. T., Christensen, T. R., Schmidt, N. M., Lund, M., Parmen-
672 tier, F.-J. W., Brown, R., Bhatt, U. S., Euskirchen, E. S., Romanovsky, V. E.,
673 et al.: Key indicators of Arctic climate change: 1971–2017, *Environ. Res. Lett.*,
674 14, 045010, <https://doi.org/10.1088/1748-9326/aafc1b>, 2019.
- 675 Bring, A., Asokan, S. M., Jaramillo, F., Jarsjö, J., Levi, L., Pietroń, J., Prieto,
676 C., Rogberg, P., and Destouni, G.: Implications of freshwater flux data from the
677 CMIP5 multimodel output across a set of Northern Hemisphere drainage basins,
678 *Earth’s Future*, 3, 206–217, <https://doi.org/10.1002/2014EF000296>, 2015.
- 679 Brodzik, M. J. and Knowles, K.: EASE-Grid: A Versatile Set of Equal-Area Pro-
680 jections and Grids, in M. Goodchild (Ed.) *Discrete Global Grids*. Santa Barbara,
681 CA, USA: National Center for Geographic Information and Analysis., 2002.
- 682 Brown, J., Jr., O. J. F., Heginbottom, J. A., and Melnikov, E. S.: Circum-Arctic
683 Map of Permafrost and Ground-Ice Conditions, Tech. rep., National Snow and Ice
684 Data Center/World Data Center for Glaciology, digital Media, revised 2001, 2001.
- 685 Burke, E. J., Zhang, Y., and Krinner, G.: Evaluating permafrost physics in the
686 Coupled Model Intercomparison Project 6 (CMIP6) models and their sensitivity
687 to climate change, *The Cryosphere*, 14, 3155–3174, <https://doi.org/10.5194/tc-14-3155-2020>, 2020.
- 689 Christensen, T. R., Johansson, T., Åkerman, H. J., Mastepanov, M., Malmer, N.,
690 Friborg, T., Crill, P., and Svensson, B. H.: Thawing sub-arctic permafrost: Ef-
691 fects on vegetation and methane emissions, *Geophys. Res. Lett.*, 31, L04501,
692 <https://doi.org/10.1029/2003GL018680>, 2004.
- 693 Clilverd, H. M., White, D. M., Tidwell, A. C., and Rawlins, M. A.: The Sensitivity of
694 Northern Groundwater Recharge to Climate Change: A Case Study in Northwest
695 Alaska, *J. Am. Water Resour. Assoc.*, pp. 1–13, <https://doi.org/10.1111/j.1752-1688.2011.00569.x>, 2011.
- 697 Connolly, C. T., Cardenas, M. B., Burkart, G. A., Spencer, R. G., and McClel-
698 land, J. W.: Groundwater as a major source of dissolved organic matter to Arc-
699 tic coastal waters, *Nat. Commun.*, 11, 1–8, <https://doi.org/10.1038/s41467-020-15250-8>, 2020.



- 701 Cooper, M. G., Zhou, T., Bennett, K. E., Bolton, W., Coon, E., Fleming, S. W., Row-
702 land, J. C., and Schwenk, J.: Detecting Permafrost Active Layer Thickness Change
703 From Nonlinear Baseflow Recession, *Water Resour. Res.*, 59, e2022WR033154,
704 <https://doi.org/10.1029/2022WR033154>, 2023.
- 705 Croghan, D., Ala-Aho, P., Lohila, A., Welker, J., Vuorenmaa, J., Kløve, B., Mus-
706 tonen, K.-R., Aurela, M., and Marttila, H.: Coupling of Water-Carbon Interac-
707 tions During Snowmelt in an Arctic Finland Catchment, *Water Resour. Res.*, p.
708 e2022WR032892, <https://doi.org/10.1029/2022WR032892>, 2023.
- 709 Cubasch, U., Meehl, G., Boer, G., Stouffer, R., Dix, M., Noda, A., Senior, C., Raper,
710 S., and Yap, K.: Projections of future climate change, chap. , in: JT Houghton,
711 Y. Ding, DJ Griggs, M. Noguer, PJ Van der Linden, X. Dai, K. Maskell, and
712 CA Johnson (eds.): *Climate Change 2001: The Scientific Basis: Contribution of*
713 *Working Group I to the Third Assessment Report of the Intergovernmental Panel*,
714 pp. 526–582, 2001.
- 715 Cucchi, M., Weedon, G. P., Amici, A., Bellouin, N., Lange, S., Müller Schmied,
716 H., Hersbach, H., and Buontempo, C.: WFDE5: bias-adjusted ERA5 re-
717 analysis data for impact studies, *Earth System Science Data*, 12, 2097–2120,
718 <https://doi.org/10.5194/essd-12-2097-2020>, 2020.
- 719 Dankers, R. and Middelkoop, H.: River discharge and freshwater runoff to the Bar-
720 ents Sea under present and future climate conditions, *Clim. Change*, 87, 131–153,
721 2008.
- 722 Dean, J., van der Velde, Y., Garnett, M. H., Dinsmore, K. J., Baxter, R., Les-
723 sels, J. S., Smith, P., Street, L. E., Subke, J.-A., Tetzlaff, D., et al.: Abun-
724 dant pre-industrial carbon detected in Canadian Arctic headwaters: implica-
725 tions for the permafrost carbon feedback, *Environ. Res. Lett.*, 13, 034024,
726 <https://doi.org/10.1088/1748-9326/aaa1fe>, 2018.
- 727 Debolskiy, M. V., Alexeev, V. A., Hock, R., Lammers, R. B., Shiklomanov, A.,
728 Schulla, J., Nicolsky, D., Romanovsky, V. E., and Prusevich, A.: Water balance
729 response of permafrost-affected watersheds to changes in air temperatures, *Envi-
730 ron. Res. Lett.*, 16, 084054, <https://doi.org/10.1088/1748-9326/ac12f3>, 2021.
- 731 Déry, S. J., Hernández-Henríquez, M. A., Burford, J. E., and Wood, E. F.:
732 Observational evidence of an intensifying hydrological cycle in northern
733 Canada, *Geophys. Res. Lett.*, 36, <https://doi.org/10.1029/2009GL038852>, L13402,
734 [doi:10.1029/2009GL038852](https://doi.org/10.1029/2009GL038852), 2009.



- 735 Du, J., Kimball, J. S., and Jones, L. A.: Passive microwave remote
736 sensing of soil moisture based on dynamic vegetation scattering prop-
737 erties for AMSR-E, *IEEE Trans. Geosci. Remote Sens.*, 54, 597–608,
738 <https://doi.org/10.1109/TGRS.2015.2462758>, 2016.
- 739 Feng, D., Gleason, C. J., Lin, P., Yang, X., Pan, M., and Ishitsuka,
740 Y.: Recent changes to Arctic river discharge, *Nat. Commun.*, 12, 6917,
741 <https://doi.org/10.1038/s41467-021-27228-1>, 2021.
- 742 Ford, V. L. and Frauenfeld, O. W.: Arctic precipitation recycling and hydrologic
743 budget changes in response to sea ice loss, *Global Planet. Change*, 209, 103752,
744 <https://doi.org/10.1016/j.gloplacha.2022.103752>, 2022.
- 745 Frey, K. E. and McClelland, J. W.: Impacts of permafrost degradation on arctic river
746 biogeochemistry, *Hydrol. Process.*, 23, 169–182, <https://doi.org/10.1002/hyp.7196>,
747 2009.
- 748 Frey, K. E. and Smith, L. C.: Amplified carbon release from vast
749 West Siberian peatlands by 2100, *Geophys. Res. Lett.*, 32, L09401,
750 <https://doi.org/10.1029/2004GL022025>, 2005.
- 751 Guo, D., Wang, A., Li, D., and Hua, W.: Simulation of Changes in the Near-Surface
752 Soil Freeze/Thaw Cycle Using CLM4.5 With Four Atmospheric Forcing Data Sets,
753 123, 2509–2523, <https://doi.org/10.1002/2017JD028097>, 2018.
- 754 Hinzman, L. D., Deal, C. J., McGuire, A. D., Mernild, S. H., Polyakov, I. V., and
755 Walsh, J. E.: Trajectory of the Arctic as an integrated system, *Ecol. Appl.*, 23,
756 1837–1868, <https://doi.org/10.1890/11-1498.1>, 2013.
- 757 Hu, Y., Ma, R., Sun, Z., Zheng, Y., Pan, Z., and Zhao, L.: Groundwater Plays an
758 Important Role in Controlling Riverine Dissolved Organic Matter in a Cold Alpine
759 Catchment, the QinghaiTibet Plateau, *Water Resour. Res.*, 59, e2022WR032426,
760 <https://doi.org/10.1029/2022WR032426>, 2023.
- 761 Hugelius, G., Tarnocai, C., Broll, G., Canadell, J., Kuhry, P., and Swanson, D.: The
762 Northern Circumpolar Soil Carbon Database: spatially distributed datasets of soil
763 coverage and soil carbon storage in the northern permafrost regions, *Earth Syst.*
764 *Sci. Data*, 5, 3–13, <https://doi.org/10.5194/essd-5-3-2013>, 2013.
- 765 Huntington, T. G.: Evidence for intensification of the global water cycle: Review and
766 synthesis, *J. Hydrol.*, 319, 83–95, <https://doi.org/10.1016/j.jhydrol.2005.07.003>,
767 2006.



- 768 Huntington, T. G.: Climate Warming-Induced Intensification of the Hydrologic Cy-
769 cle: An Assessment of the Published Record and Potential Impacts on Agricul-
770 ture, *Adv. Agron.*, 109, 1–53, [https://doi.org/10.1016/B978-0-12-385040-9.00001-](https://doi.org/10.1016/B978-0-12-385040-9.00001-3)
771 3, 2010.
- 772 Jin, H., Huang, Y., Bense, V. F., Ma, Q., Marchenko, S. S., Shepelev, V. V., Hu, Y.,
773 Liang, S., Spektor, V. V., Jin, X., Li, X., and Li, X.: Permafrost Degradation and
774 Its Hydrogeological Impacts, *Water*, 14, 372, <https://doi.org/10.3390/w14030372>,
775 2022.
- 776 Jones, B. M., Grosse, G., Farquharson, L. M., Roy-Léveillé, P., Veremeeva, A.,
777 Kanevskiy, M. Z., Gaglioti, B. V., Breen, A. L., Parsekian, A. D., Ulrich, M.,
778 et al.: Lake and drained lake basin systems in lowland permafrost regions, *Nat.*
779 *Rev. Earth Environ.*, 3, 85–98, <https://doi.org/10.1038/s43017-021-00238-9>, 2022.
- 780 Koch, J. C., Bogard, M. J., Butman, D. E., Finlay, K., Ebel, B., James, J., John-
781 ston, S. E., Jorgenson, M. T., Pastick, N. J., Spencer, R. G., et al.: Heterogeneous
782 Patterns of Aged Organic Carbon Export Driven by Hydrologic Flow Paths, Soil
783 Texture, Fire, and Thaw in Discontinuous Permafrost Headwaters, *Global Bio-*
784 *geochem. Cy.*, 36, e2021GB007242, <https://doi.org/10.1029/2021GB007242>, 2022.
- 785 Koven, C. D., Riley, W. J., and Stern, A.: Analysis of Permafrost Thermal Dynamics
786 and Response to Climate Change in the CMIP5 Earth System Models, *J. Climate*,
787 26, 1877–1900, <https://doi.org/10.1175/JCLI-D-12-00228.1>, 2013.
- 788 Lafrenière, M. J. and Lamoureux, S. F.: Effects of changing permafrost condi-
789 tions on hydrological processes and fluvial fluxes, *Earth-Sci. Rev.*, 191, 212–223,
790 <https://doi.org/10.1016/j.earscirev.2019.02.018>, 2019.
- 791 Lange, S.: Trend-preserving bias adjustment and statistical downscal-
792 ing with ISIMIP3BASD (v1. 0), *Geosci. Model Dev.*, 12, 3055–3070,
793 <https://doi.org/10.5194/gmd-12-3055-2019>, 2019.
- 794 Lange, S.: ISIMIP3BASD, <https://doi.org/10.5281/zenodo.4686991>, 2021.
- 795 Lange, S., Menz, C., Gleixner, S., Cucchi, M., Weedon, G. P., Amici, A., Bel-
796 louin, N., Schmied, H. M., Hersbach, H., Buontempo, C., and Cagnazzo,
797 C.: WFDE5 over land merged with ERA5 over the ocean (W5E5 v2.0),
798 <https://doi.org/10.48364/ISIMIP.342217>, 2021.



- 799 Lawrence, D. M. and Slater, A. G.: Incorporating organic soil into a global climate
800 model, *Clim. Dynam.*, 30, 145–160, <https://doi.org/10.1007/s00382-007-0278-1>,
801 2008.
- 802 Liljedahl, A. K., Boike, J., Daanen, R. P., Fedorov, A. N., Frost, G. V., Grosse, G.,
803 Hinzman, L. D., Iijma, Y., Jorgenson, J. C., Matveyeva, N., et al.: Pan-Arctic ice-
804 wedge degradation in warming permafrost and its influence on tundra hydrology,
805 *Nat. Geosci.*, 9, 312–318, <https://doi.org/10.1038/ngeo2674>, 2016.
- 806 Liston, G. E., Haehnel, R. B., Sturm, M., Hiemstra, C. A., Bere-
807 zovskaya, S., and Tabley, R. D.: Simulating complex snow distribu-
808 tions in windy environments using SnowTran-3D, *J. Glaciol.*, 53, 241–256,
809 <https://doi.org/10.3189/172756507782202865>, 2007.
- 810 Liu, S., Wang, P., Yu, J., Wang, T., Cai, H., Huang, Q., Pozdniakov, S. P., Zhang,
811 Y., and Kazak, E. S.: Mechanisms behind the uneven increases in early, mid-and
812 late winter streamflow across four Arctic river basins, *J. Hydrol.*, 606, 127425,
813 <https://doi.org/10.1016/j.jhydrol.2021.127425>, 2022.
- 814 Martens, B., Miralles, D. G., Lievens, H., Van Der Schalie, R., De Jeu, R. A.,
815 Fernández-Prieto, D., Beck, H. E., Dorigo, W. A., and Verhoest, N. E.: GLEAM
816 v3: satellite-based land evaporation and root-zone soil moisture, *Geosci. Model*
817 *Dev.*, 10, 1903–1925, <https://doi.org/10.5194/gmd-10-1903-2017>, 2017.
- 818 McClelland, J. W., Holmes, R. M., Peterson, B. J., and Stieglitz, M.: Increasing
819 river discharge in the Eurasian Arctic: Consideration of dams, permafrost thaw,
820 and fires as potential agents of change, *J. Geophys. Res.-Atmos.*, 109, D18102,
821 <https://doi.org/10.1029/2004JD004583>, 2004.
- 822 McClelland, J. W., Déry, S. J., Peterson, B. J., Holmes, R. M., and Wood, E. F.: A
823 pan-arctic evaluation of changes in river discharge during the latter half of the 20th
824 century, *Geophys. Res. Lett.*, 33, L06715, <https://doi.org/10.1029/2006GL025753>,
825 2006.
- 826 McCrystall, M. R., Stroeve, J., Serreze, M., Forbes, B. C., and Screen, J. A.: New
827 climate models reveal faster and larger increases in Arctic precipitation than pre-
828 viously projected, *Nat. Commun.*, 12, 6765, <https://doi.org/10.1038/s41467-021-27031-y>, 2021.
- 830 McKenzie, J. M., Kurylyk, B. L., Walvoord, M. A., Bense, V. F., Fortier, D., Spence,
831 C., and Grenier, C.: Invited perspective: What lies beneath a changing Arctic?,
832 *The Cryosphere*, 15, 479–484, <https://doi.org/10.5194/tc-15-479-2021>, 2021.



- 833 Miralles, D. G., Holmes, T., De Jeu, R., Gash, J., Meesters, A., and Dolman,
834 A.: Global land-surface evaporation estimated from satellite-based observations,
835 Hydrol. Earth Syst. Sci., 15, 453–469, <https://doi.org/10.5194/hess-15-453-2011>,
836 2011.
- 837 Mohammed, A. A., Guimond, J. A., Bense, V. F., Jamieson, R. C., McKenzie, J. M.,
838 and Kurylyk, B. L.: Mobilization of subsurface carbon pools driven by permafrost
839 thaw and reactivation of groundwater flow: a virtual experiment, Environ. Res.
840 Lett., 17, 124 036, <https://doi.org/10.1088/1748-9326/aca701>, 2022.
- 841 Nash, D., Waliser, D., Guan, B., Ye, H., and Ralph, F. M.: The Role of Atmospheric
842 Rivers in Extratropical and Polar Hydroclimate, J. Geophys. Res.-Atmos., 123,
843 6804–6821, <https://doi.org/10.1029/2017JD028130>, 2018.
- 844 Ni, J., Wu, T., Zhu, X., Hu, G., Zou, D., Wu, X., Li, R., Xie, C., Qiao, Y., Pang,
845 Q., et al.: Simulation of the Present and Future Projection of Permafrost on the
846 Qinghai-Tibet Plateau with Statistical and Machine Learning Models, J. Geophys.
847 Res.-Atmos., 126, e2020JD033 402, <https://doi.org/10.1029/2020JD033402>, 2021.
- 848 Nicolsky, D., Romanovsky, V., Alexeev, V., and Lawrence, D.: Improved modeling
849 of permafrost dynamics in a GCM land-surface scheme, Geophys. Res. Lett., 34,
850 L08 501, <https://doi.org/10.1029/2007GL029525>, 2007.
- 851 Overland, J., Dunlea, E., Box, J. E., Corell, R., Forsius, M., Kattsov, V., Olsen,
852 M. S., Pawlak, J., Reiersen, L.-O., and Wang, M.: The urgency of Arctic change,
853 Polar Sci., 21, 6–13, <https://doi.org/10.1016/j.polar.2018.11.008>, 2019.
- 854 Painter, S. L., Coon, E. T., Khattak, A. J., and Jastrow, J. D.: Drying of tundra
855 landscapes will limit subsidence-induced acceleration of permafrost thaw, Proc.
856 Natl. Acad. Sci., 120, e2212171 120, <https://doi.org/10.1073/pnas.22121711>, 2023.
- 857 Peng, X., Zhang, T., Frauenfeld, O. W., Wang, K., Luo, D., Cao, B., Su, H., Jin, H.,
858 and Wu, Q.: Spatiotemporal Changes in Active Layer Thickness under Contempo-
859 rary and Projected Climate in the Northern Hemisphere, J. Climate, 31, 251–266,
860 <https://doi.org/10.1175/JCLI-D-16-0721.1>, 2018.
- 861 Peterson, B. J., Holmes, R. M., McClelland, J. W., Vörösmarty, C. J., Lam-
862 mers, R. B., Shiklomanov, A. I., Shiklomanov, I. A., and Rahmstorf, S.:
863 Increasing River Discharge to the Arctic Ocean, Science, 298, 2171–2173,
864 <https://doi.org/10.1126/science.1077445>, 2002.



- 865 Ran, Y., Li, X., Cheng, G., Che, J., Aalto, J., Karjalainen, O., Hjort, J., Luoto, M.,
866 Jin, H., Obu, J., et al.: New high-resolution estimates of the permafrost thermal
867 state and hydrothermal conditions over the Northern Hemisphere, *Earth Syst. Sci.*
868 *Data*, 14, 865–884, <https://doi.org/10.5194/essd-14-865-2022>, 2022.
- 869 Rantanen, M., Karpechko, A. Y., Lipponen, A., Nordling, K., Hyvärinen, O., Ru-
870 osteenoja, K., Vihma, T., and Laaksonen, A.: The Arctic has warmed nearly
871 four times faster than the globe since 1979, *Commun. Earth Environ.*, 3, 168,
872 <https://doi.org/10.1038/s43247-022-00498-3>, 2022.
- 873 Rawlins, M. A.: Increasing freshwater and dissolved organic carbon flows
874 to Northwest Alaskas Elson lagoon, *Environ. Res. Lett.*, 16, 105014,
875 <https://doi.org/10.1088/1748-9326/ac2288>, 2021.
- 876 Rawlins, M. A., Lammers, R. B., Froking, S., Fekete, B. M., and Vörösmarty,
877 C. J.: Simulating Pan-Arctic Runoff with a Macro-Scale Terrestrial Water Bal-
878 ance Model, *Hydrol. Process.*, 17, 2521–2539, <https://doi.org/10.1002/hyp.1271>,
879 2003.
- 880 Rawlins, M. A., Steele, M., Holland, M. M., Adam, J. C., Cherry, J. E.,
881 Francis, J. A., Groisman, P. Y., Hinzman, L. D., Huntington, T. G., Kane,
882 D. L., and Coauthors: Analysis of the Arctic System for Freshwater Cy-
883 cle Intensification: Observations and Expectations, *J. Climate*, 23, 5715–5737,
884 <https://doi.org/10.1175/2010JCLI3421.1>, 2010.
- 885 Rawlins, M. A., Nicolsky, D. J., McDonald, K. C., and Romanovsky, V. E.: Simulat-
886 ing soil freeze/thaw dynamics with an improved pan-Arctic water balance model,
887 *J. Adv. Model. Earth Sys.*, 5, 659–675, <https://doi.org/10.1002/jame.20045>, 2013.
- 888 Rawlins, M. A., Cai, L., Stuefer, S. L., and Nicolsky, D. J.: Changing characteristics
889 of runoff and freshwater export from watersheds draining northern Alaska, *The*
890 *Cryosphere*, 13, 3337–3352, <https://doi.org/10.5194/tc-13-3337-2019>, 2019.
- 891 Rawlins, M. A., Connolly, C. T., and McClelland, J. W.: Modeling Terrestrial Dis-
892 solved Organic Carbon Loading to Western Arctic Rivers, *J. Geophys. Res.-Biogeo*,
893 126, e2021JG006420, <https://doi.org/10.1029/2021JG006420>, 2021.
- 894 Sazonova, T. S. and Romanovsky, V. E.: A model for regional-scale
895 estimation of temporal and spatial variability of active layer thickness
896 and mean annual ground temperatures, *Permafrost Periglac.*, 14, 125–139,
897 <https://doi.org/10.1002/ppp.449>, 2003.



- 898 Schroeder, R., McDonald, K. C., Zimmerman, R., Podest, E., and Rawlins, M.:
899 North Eurasian Inundation Mapping with Passive and Active Microwave Remote
900 Sensing, *Environ. Res. Lett.*, 5, 015003, <https://doi.org/10.1088/1748-9326>, 2010.
- 901 Schwab, M. S., Hilton, R. G., Raymond, P. A., Haghypour, N., Amos, E., Tank, S. E.,
902 Holmes, R. M., Tipper, E. T., and Eglinton, T. I.: An Abrupt Aging of Dissolved
903 Organic Carbon in Large Arctic Rivers, *Geophys. Res. Lett.*, 47, e2020GL088823,
904 <https://doi.org/10.1029/2020GL088823>, 2020.
- 905 Serreze, M. C. and Meier, W. N.: The Arctic's sea ice cover: trends, variability,
906 predictability, and comparisons to the Antarctic, *Ann. N. Y. Acad. Sci.*, 1436,
907 36–53, <https://doi.org/10.1111/nyas.13856>, 2019.
- 908 Shapiro, S. S. and Wilk, M. B.: An analysis of variance test for normality (complete
909 samples), *Biometrika*, 52, 591–611, <https://doi.org/10.2307/2333709>, 1965.
- 910 Shiklomanov, A. I., Lammers, R. B., Lettenmaier, D. P., Polischuk, Y. M., Savichev,
911 O. G., Smith, L. C., and Chernokulsky, A. V.: Hydrological Changes: His-
912 torical Analysis, Contemporary Status, and Future Projections, Regional En-
913 vironmental Changes in Siberia and Their Global Consequences, pp. 111–154,
914 https://doi.org/10.1007/978-94-007-4569-8_4, 2013.
- 915 Shiklomanov, I. A. and Shiklomanov, A. I.: Climatic Change and Dynamics of River
916 Discharge into the Arctic Ocean, *Water Resources*, 30, 593–601, 2003.
- 917 Shiklomanov, I. A., Shiklomanov, A. I., Lammers, R. B., Peterson, B. J., and Vörös-
918 marty, C. J.: The dynamics of river water inflow to the Arctic Ocean, pp. 281–296,
919 Kluwer Academic Press, Dordrecht, in *The Freshwater Budget of the Arctic Ocean*,
920 edited by E.I Lewis, et al., 2000.
- 921 Sjöberg, Y., Jan, A., Painter, S. L., Coon, E. T., Carey, M. P., O'Donnell,
922 J. A., and Koch, J. C.: Permafrost Promotes Shallow Groundwater Flow
923 and Warmer Headwater Streams, *Water Resour. Res.*, 57, e2020WR027463,
924 <https://doi.org/10.1029/2020WR027463>, 2021.
- 925 Slater, A. G. and Lawrence, D. M.: Diagnosing Present and Future Permafrost from
926 Climate Models, *J. Climate*, 26, 5608–5623, <https://doi.org/10.1175/JCLI-D-12-00341.1>, 2013.
- 928 Smith, L. C., Sheng, Y., MacDonald, G. M., and Hinzman, L. D.: Disappearing
929 Arctic Lakes, *Science*, 308, p. 1429, <https://doi.org/10.1029/2004JD005518>, 2005.



- 930 Spencer, R. G., Mann, P. J., Dittmar, T., Eglinton, T. I., McIntyre, C.,
931 Holmes, R. M., Zimov, N., and Stubbins, A.: Detecting the signature
932 of permafrost thaw in Arctic rivers, *Geophys. Res. Lett.*, 42, 2830–2835,
933 <https://doi.org/10.1002/2015GL063498>, 2015.
- 934 St. Jacques, J. M. and Sauchyn, D. J.: Increasing winter baseflow and mean annual
935 streamflow from possible permafrost thawing in the Northwest Territories, Canada,
936 *Geophys. Res. Lett.*, 36, L01401, <https://doi.org/10.1029/2008GL035822>, 2009.
- 937 Streletskiy, D. A., Tananaev, N. I., Opel, T., Shiklomanov, N. I., Nyland,
938 K. E., Streletskaya, I. D., Shiklomanov, A. I., et al.: Permafrost hydrology
939 in changing climatic conditions: seasonal variability of stable isotope compo-
940 sition in rivers in discontinuous permafrost, *Environ. Res. Lett.*, 10, 095003,
941 <https://doi.org/10.1088/1748-9326/10/9/095003>, 2015.
- 942 Striegl, R. G., Aiken, G. R., Dornblaser, M. M., Raymond, P. A., and Wick-
943 land, K. P.: A decrease in discharge-normalized DOC export by the Yukon
944 River during summer through autumn, *Geophys. Res. Lett.*, 32, L21413,
945 <https://doi.org/10.1029/2005GL024413>, 2005.
- 946 Stroeve, J. and Notz, D.: Changing state of Arctic sea ice across all seasons, *Environ.*
947 *Res. Lett.*, 13, 103001, <https://doi.org/10.1088/1748-9326/aade56>, 2018.
- 948 Sturm, M. J., Holmgren, J., and Liston, G. E.: A Seasonal Snow Cover Clas-
949 sification System for Local to Global Applications, *J. Climate*, 8, 1261–1283,
950 [https://doi.org/10.1175/1520-0442\(1995\)008<1261:ASSCCS>2.0.CO;2](https://doi.org/10.1175/1520-0442(1995)008<1261:ASSCCS>2.0.CO;2), 1995.
- 951 Tananaev, N., Makarieva, O., and Lebedeva, L.: Trends in annual and extreme flows
952 in the Lena River basin, Northern Eurasia, *Geophys. Res. Lett.*, 43, 10764–10772,
953 <https://doi.org/10.1002/2016GL070796>, 2016.
- 954 Tananaev, N., Teisserenc, R., and Debolskiy, M.: Permafrost Hydrol-
955 ogy Research Domain: Process-Based Adjustment, *Hydrology*, 7, 6,
956 <https://doi.org/10.3390/hydrology7010006>, 2020.
- 957 Tank, S. E., Striegl, R. G., McClelland, J. W., and Kokelj, S. V.: Multi-decadal
958 increases in dissolved organic carbon and alkalinity flux from the Macken-
959 zie drainage basin to the Arctic Ocean, *Environ. Res. Lett.*, 11, 054015,
960 <https://doi.org/10.1088/1748-9326/11/5/054015>, 2016.



- 961 Wagner, A., Lohmann, G., and Prange, M.: Arctic river dis-
962 charge trends since 7 ka BP, *Global Planet. Change*, 79, 48–60,
963 <https://doi.org/10.1016/j.gloplacha.2011.07.006>, 2011.
- 964 Walsh, J. E., Chapman, W. L., Romanovsky, V., Christensen, J. H., and Stendel,
965 M.: Global climate model performance over Alaska and Greenland, *J. Climate*,
966 21, 6156–6174, <https://doi.org/10.1175/2008JCLI2163.1>, 2008.
- 967 Walvoord, M. A. and Kurylyk, B. L.: Hydrologic impacts of thawing
968 permafrost—A review, *Vadose Zone J.*, 15, vzj2016.01.0010,
969 <https://doi.org/10.2136/vzj2016.01.0010>, 2016.
- 970 Walvoord, M. A. and Striegl, R. G.: Increased groundwater to stream dis-
971 charge from permafrost thawing in the Yukon River basin: Potential impacts
972 on lateral export of carbon and nitrogen, *Geophys. Res. Lett.*, 34, L12402,
973 <https://doi.org/10.1029/2007GL030216>, 2007.
- 974 Wang, P., Huang, Q., Pozdniakov, S. P., Liu, S., Ma, N., Wang, T., Zhang, Y., Yu,
975 J., Xie, J., Fu, G., et al.: Potential role of permafrost thaw on increasing Siberian
976 river discharge, *Environ. Res. Lett.*, 16, 034046, <https://doi.org/10.1088/1748-9326/abe326>, 2021.
- 978 Wang, Y.-R., Hessen, D. O., Samset, B. H., and Stordal, F.: Evaluating global
979 and regional land warming trends in the past decades with both MODIS and
980 ERA5-Land land surface temperature data, *Remote Sens. Environ.*, 280, 113181,
981 <https://doi.org/10.1016/j.rse.2022.113181>, 2022.
- 982 Warszawski, L., Frieler, K., Huber, V., Piontek, F., Serdeczny, O.,
983 and Schewe, J.: The inter-sectoral impact model intercomparison project
984 (ISI-MIP): project framework, *Proc. Natl. Acad. Sci.*, 111, 3228–3232,
985 <https://doi.org/10.1073/pnas.131233011>, 2014.
- 986 Woo, M.-K., Kane, D. L., Carey, S. K., and Yang, D.: Progress in per-
987 mafrost hydrology in the new millennium, *Permafrost Periglac.*, 19, 237–254,
988 <https://doi.org/10.1002/ppp.613>, 2008.
- 989 Yi, Y., Chen, R. H., Kimball, J. S., Moghaddam, M., Xu, X., Euskirchen, E. S., Das,
990 N., and Miller, C. E.: Potential Satellite Monitoring of Surface Organic Soil Prop-
991 erties in Arctic Tundra From SMAP, *Water Resour. Res.*, 58, e2021WR030957,
992 <https://doi.org/10.1029/2021WR030957>, 2022.



- 993 Zhang, K., Kimball, J. S., Mu, Q., Jones, L. A., Goetz, S. J., and Running,
994 S. W.: Satellite based analysis of northern ET trends and associated changes
995 in the regional water balance from 1983 to 2005, *J. Hydrol.*, 379, 92–110,
996 <https://doi.org/10.1016/j.jhydrol.2009.09.047>, 2009.
- 997 Zhang, P., Chen, G., Ting, M., Ruby Leung, L., Guan, B., and Li, L.: More frequent
998 atmospheric rivers slow the seasonal recovery of Arctic sea ice, *Nat. Clim. Change.*,
999 13, 266–273, <https://doi.org/10.1038/s41558-023-01599-3>, 2023.
- 1000 Zhang, S.-M., Mu, C.-C., Li, Z.-L., Dong, W.-W., Wang, X.-Y., Strelet-
1001 skaya, I., Grebenets, V., Sokratov, S., Kizyakov, A., and Wu, X.-D.:
1002 Export of nutrients and suspended solids from major Arctic rivers and
1003 their response to permafrost degradation, *Adv. Clim. Chang.*, 12, 466–474,
1004 <https://doi.org/10.1016/j.accre.2021.06.002>, 2021.
- 1005 Zhang, X., He, J., Zhang, J., Polyakov, I., Gerdes, R., Inoue, J., and Wu, P.: En-
1006 hanced poleward moisture transport and amplified northern high-latitude wetting
1007 trend, *Nat. Clim. Change.*, 3, 47–51, <https://doi.org/10.1038/nclimate1631>, 2013.